# Surface Modification of 316L Stainless Steel for Carbon Nanotube Growth

Michael Manwaring

A senior thesis submitted to the faculty of
Brigham Young University
in partial fulfillment of the requirements for the degree of

Bachelor of Science

Felipe Rivera, Richard Vanfleet and Brian Jensen, Advisors

Department of Physics and Astronomy

Brigham Young University

December 16, 2021

ABSTRACT

Surface Modification of 316L Stainless Steel for Carbon Nanotube Growth

Michael Manwaring

Department of Physics and Astronomy

Bachelor of Science

The purpose of this research is to study the mechanism that promotes carbon nanotube (CNT) growth on 316L stainless steel upon annealing. The annealing process physically alters the surface structure and composition of the material. For various times in air and argon atmosphere, the stainless steel (SS) is heated to 800°C. The surface structure is compared between the various samples. Among the most notable characteristics is the growth of faceted surface nodules that appear crystalline and apparent grain boundaries separating areas of pronounced and minimal growth. Scanning electron microscopy (SEM) and energy-dispersive X-ray spectroscopy (EDX) are used for the initial analysis of morphological and compositional surface changes. Focused ion beam (FIB) cross sections were lifted out to further study the surface changes with transmission electron microscopy (TEM). It is shown that a continuous surface layer forms on the 316L stainless steel upon heat treatment in air and argon. Furthermore, the surface layer is not dependent on air for apparent nodule formation. This top layer is also shown not to have existed on the stainless steel in its initial condition. Using EDX analysis, it is also observed that the surface layer has no nickel, while iron and chromium appear to have diffused into this region. Additionally, there appears to be a significant amount of oxygen in the surface layer prior to CNT growth. After undergoing heat treatment in ethylene, the surface layer is found with TEM to become discontinuous and reduced of its oxygen. Carbon nanotubes are found to grow from these congregated sites.

Keywords: CNT, stainless steel, annealing, EDX, SEM/TEM

# ACKNOWLEDGMENTS

This research would not have been possible without the valuable help of several individuals. I would like to thank my family for their love and support throughout the years as I went back to school, particularly my brother. I would also like to thank Sarah for her patient support. She often voiced faith in me though I didn't have faith in myself.

I would like to acknowledge the guidance of my advisor, Dr Felipe Rivera, and thank him for his willingness to take me on and guide me through the process of writing. I would also like to thank him for his council and direction in helping me graduate. This would not have been possible without his help.

Thanks also to Drs. Richard Vanfleet and Brian Jensen for meeting with me and offering their input and encouragement. Their expertise was invaluable.

I also want to acknowledge and thank various staff who helped with training and instruction on the processes and equipment necessary to do this research. Among them are Paul Minson, who offered his expertise in helping me attain TEM data as well as training me on the SEM and EDX, Michael Standing, who instructed me in the use of the FIB, and Nick Allen, who trained me in the use of the CNT furnace.

# Contents

# List of Figures

# List of Tables

# 1 Introduction

## 1.1 Motivation

The purpose of this thesis is to examine the surface modification that allows for carbon nanotube (CNT) growth on stainless steel. This process is not sufficiently understood. CNTs require a catalyst, such as iron nanoparticles, to begin growing. 316L stainless steel that has not undergone heat treatment does not readily grow carbon nanotubes (Zhuo, 2014). In examining the surface modification of the stainless steel, we hope to determine what possible processes could give rise to a nucleating agent.

The reason this is important is because CNT coated surfaces have applications in medicine. Medical equipment can be treated with CNTs which act as a barrier to bacterial growth. This allows for use in the body without chemical sterilization. Mechanical resistance to bacterial growth has advantages over chemical resistance because it is much more difficult for microbes to develop immunity to physical barriers (Voss, 2021). Unfortunately, there are some problems

associated with CNT coated surfaces. Understanding the process may help us mitigate those problems and lead to an eventual solution.

## 1.2 Background

Post operative infection is a major area of concern in the medical industry. Certain microbes and the threat they pose are of particular concern. Among these are Staphylococcus aureus and Escherichia coli. These pose a serious concern because of their resistance to various drugs (Morco,2021). The problem is microbes develop chemical resistance through adaptation and evolution. Chemical resistance is achieved as the organism changes chemical characteristics within its body that help it cope with its environment. Even with responsible practices, bacteria are, over time, able to develop resistance.

Medical devices must be treated with chemical antibiotics to sterilize them for use in the human body. This includes scalpels and other tools, as well as implants and prosthetics. These surfaces need to be virtually free of any sort of biofilm or they pose a serious threat to the health of the patient. One possible and promising solution to the use of chemical agents for fighting bacterial proliferation is the use of mechanical agents (Morco,2021).

Unlike chemical means, it is much more difficult for microbes to develop an adaptation to a mechanical hinderance. It would typically take much more than a chemical adaptation to deal with such an inhospitable environment (Voss, 2021). One such environment is a surface treated with carbon nanotubes (CNTs).

It has been shown that carbon nanotubes show a significant hinderance to the proliferation of drug resistant bacteria (Morco, 2021). They have been tested on silicon as well as stainless steel surfaces**.** The purpose of this paper is to determine the surface structure of heat treated 316L stainless steel. We attempt to determine the mechanism that catalyzes nucleation of

CNTs on stainless steel and what this may be able to tell us about how to address various issues that come with using stainless steel in the body. It is our hypothesis that this nucleation agent of carbon nanotubes on stainless steel is iron that has been reduced from iron oxides on the surface of the stainless-steel substrate.

Dr Zhuo et al. (2014) published a paper examining the processes associated with carbon nanotube growth on 316L stainless steel. They hypothesized that the carbon nanotubes grew from iron particles on the surface that were reduced during the growth phase of the CNTs. They also state that the structure on the surface of the stainless-steel substrate is primarily chromium oxide.

They found that surface roughness and size of nodule were both affected by heat treatments. This in turn influences the size of carbon nanotubes that grow on the surface. They found that the most energetic growth occurs with air heat treatments of 10 or fewer minutes. They also observed the most aligned growth, with nanotubes extending perpendicular to the surface, at 10 minutes, but not at other times. Nanotube growth diminished and ceased for heat treatments longer than 20 minutes. Though, it is the opinion of this paper that the source of catalyzation appears to be inconclusive and worthy of further study.

## 1.3 Previous Research at BYU

Stephanie Morco and Sterling Voss have also done some analysis of CNTs on 316L at Brigham Young University. Morco (2021) examined the bacterial resistance of carbon infiltrated carbon nanotube (CICNT) forests. Samples in this study were heat treated for various times between 1.5 and 30 minutes in air. Samples were prepared both for flat surfaces and rounded surfaces to observe differences in surface morphology. The results of the study partially agree

with those of Zhuo et. al. (2014). Namely, short heat treatments yield non-unform particles, and long, over 10-minute, heat treatments yield particles that are too large. This study found that a 2-minute heat treatment was ideal. It gave uniform particle size that was in the 100 nm range.

Though the particles were the target size, the resulting carbon nanotube forests were not aligned. Also, the carbon nanotubes here are about ten times thicker than those in the Zhuo experiment. It is not clear as to why. Additionally, there is some ambiguity in the two studies concerning what is the best method to achieve vertically aligned growth. Zhuo et. al suggested 10 minutes gave these results while Morco suggested 2 minutes.

Voss (2021) further investigated the effect that carbon infiltrated carbon nanotube growth has on the biocompatibility of 316L stainless steel. On various samples CNTs were grown in a furnace. These samples were tested for corrosion resistance, as well as tested against the corrosive resistance of the control sample. The samples with CNTs showed corrosion when put in saline solution, but the control did not. While there is a definite chemical change that the carbon nanotubes had on the surface, the source of the corrosion is still unexplained.

This raises several questions. What is the source of the corrosion? How does the growth of carbon nanotubes affect the material makeup of the surface that makes it susceptible to corrosion? Is there a way to mitigate these effects? We need to address these issues if these materials are to be a viable option for use in medical applications.

## 1.4 Overview

The primary objective of this thesis is to determine the catalyst for nucleation of CNTs on 316L stainless steel. CNTs do not grow on 316L stainless steel prior to the annealing process.

We hypothesize that the CNTs are growing on iron that has either migrated to the surface during the heating process or reduced by hydrogen present in ethylene gas during the growth phase.

This thesis analyzes and compares several samples of stainless steel which have undergone annealing in various environments. We recreate conditions that previously were shown by Zhuo, Morco, and Voss to promote nanotube growth, and examine others to determine baseline parameters.

We prepare 12 samples heated in air and argon for times varying between one, two and four minutes in air and five, ten, and twenty minutes in argon (refer to appendix B for an index of sample number and processing characteristics). All samples that undergo annealing show growth of faceted nodules that appear crystalline on the surface. It was also observed that the stainless-steel grain structure was still present in the nodule formation, with variation in grain size between grains.

There were two samples that were promising for this study: Sample 3 was heated for four minutes in air and Sample 12 was heated for four minutes in air, followed by twenty minutes in argon. We used energy-dispersive x-ray spectroscopy (EDX) analysis to characterize the features observed post-treatment. Additional samples, prepared using the same processing recipe as samples 3 and 12, demonstrated CNT growth achieved post heat-treatment by an in-situ 15-minute flow of ethylene.

Samples 3, 12 and 15 (sample 3 with CNT processing), and a control sample were then selected for additional analysis via transmission electron microscopy (TEM). Cross-sections of the surface from these samples were extracted and prepared using a focused ion beam (FIB) method and EDX analysis was performed on these in the TEM.

# 2 Methods

This chapter contains information concerning the surface modification of stainless steel, CNT growth on the surface, and surface characterization. Following the description of sample preparation, procedures concerning the analysis are described.

## 2.1 Equipment

The equipment used in this research comprised of a furnace for growing the CNTs and three electron microscopes. One scanning electron microscope (SEM), also called the Verios, was used to do EDX analysis. An SEM/FIB dual beam, the Helios, was used for preparing samples for the TEM using a Focused Ion Beam (FIB).


**Figure 2.1** Verios SEM (left) and Helios SEM/FIB (right).

## 2.2 Annealing and CNT Growth

In his work, Sterling Voss presented three procedures for growing CNTs on stainless steel. Procedure A, previously developed, consisted of inserting and removing the sample twice for each growth and was time intensive. Procedure B consisted of changing temperatures between different atmospheres. Ultimately, he developed growth procedure C because it was effective in growing CNTs while also being more efficient (Voss, 2021).

Growth Procedure C is as follows:

1. Samples are placed in a furnace preheated to 800◦C with air flowing for a 2-minute heat treatment.
2. Flow is changed from air to argon for an additional 10-minute heat treatment.
3. Samples are subjected to flowing argon and ethylene at 800◦C for a 20-minute growth.
4. Flow is restricted to argon as the furnace is heated to 900◦C.
5. Samples are subjected to flowing argon and ethylene at 900◦C for a 10-minute infiltration.
6. Flow is again restricted to just argon as the furnace is cooled to room temperature and the samples are removed.

In this work, we follow a similar procedure to Growth Procedure C, but without the carbon infiltration. We annealed for various times in air and argon to determine differences in surface structure. After analysis of the surfaces, it was determined to prepare a sample to minimize oxidation on the surface. This was done with an anneal in argon only and with a reduction followed by an anneal in argon. We also prepared samples with CNT growth following Sterling Voss' aforementioned procedure C.

The following are the various annealing and growth procedures.

### 2.2.1 Annealing Procedure 1

1. Samples are placed in a furnace preheated to 800°C and allowed to come to temperature while air is flowing.

2. Respective samples dwell for 1, 2, or 4 minutes with air flowing.

3. Samples are pulled to the end of the furnace tube to sit for 2 minutes before being taken out (See Figure 2.2).

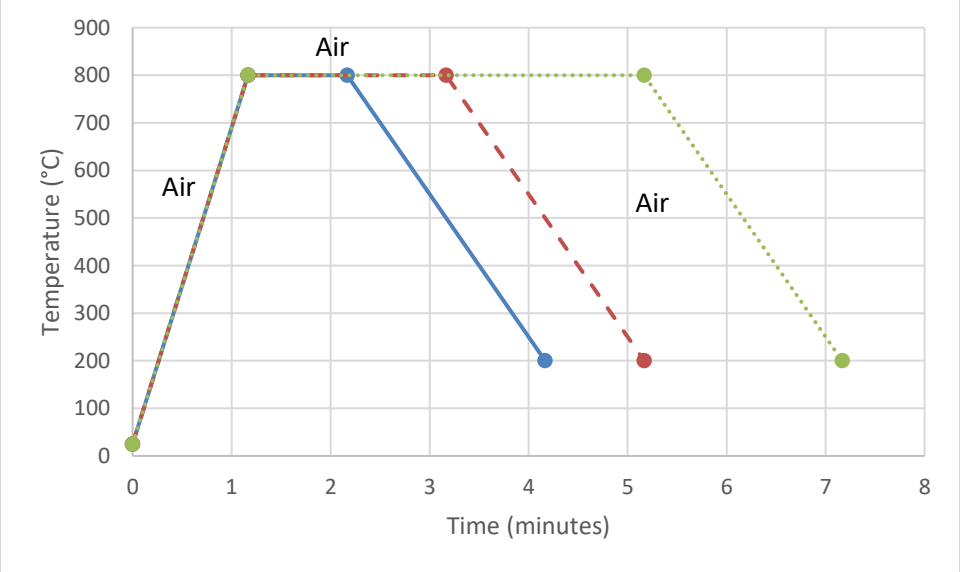


**Figure 2.2** Heat treatments for samples 1, 2, and 3. Samples placed in a pre-heated 800°C air environment for 1, 2, and 4 minutes (respectively).

### 2.2.2 Annealing Procedure 2

1. Samples are placed in a furnace preheated to 800°C and allowed to come to temperature while air is flowing.

2. Respective samples dwell for 1, 2, or 4 minutes with air flowing.

3. Flow is changed from air to argon for an additional **5-minute** heat treatment.

4. Still flowing argon, the furnace is cooled to 200°C and the samples are removed (See Figure 2.3).

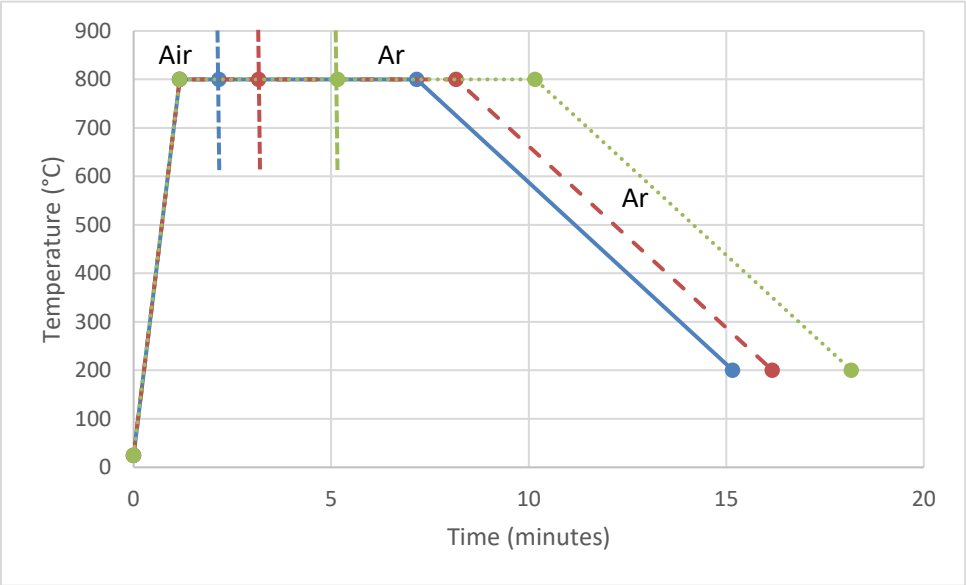


**Figure 2.3** Heat treatments for samples 4, 5, and 6. Samples placed in a pre-heated 800°C air environment for 1, 2, and 4 minutes (respectively), then for 5 minutes in argon.

### 2.2.3 Annealing Procedure 3

Annealing Procedure 3 is the same as Annealing Procedure 2, but with a **10-minute** dwell in argon in step 3 (See Figure 2.4).

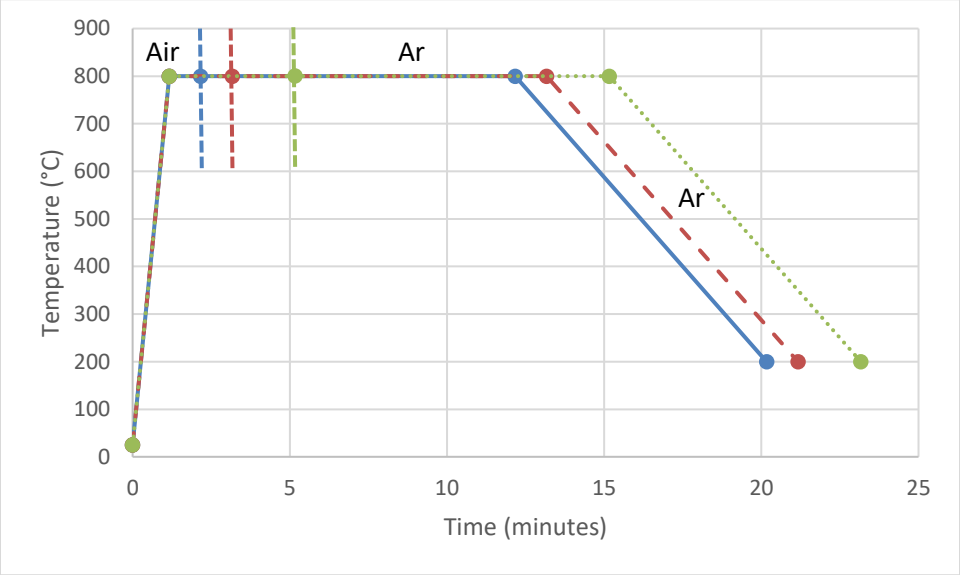


**Figure 2.4** Heat treatments for samples 7, 8, and 9. Samples placed in a pre-heated 800°C air environment for 1, 2, and 4 minutes (respectively), then for 10 minutes in argon.

### 2.2.4 Annealing Procedure 4

Annealing Procedure 4 is the same as Annealing Procedure 2, but with a **20-minute** dwell in argon in step 3 (See Figure 2.5).

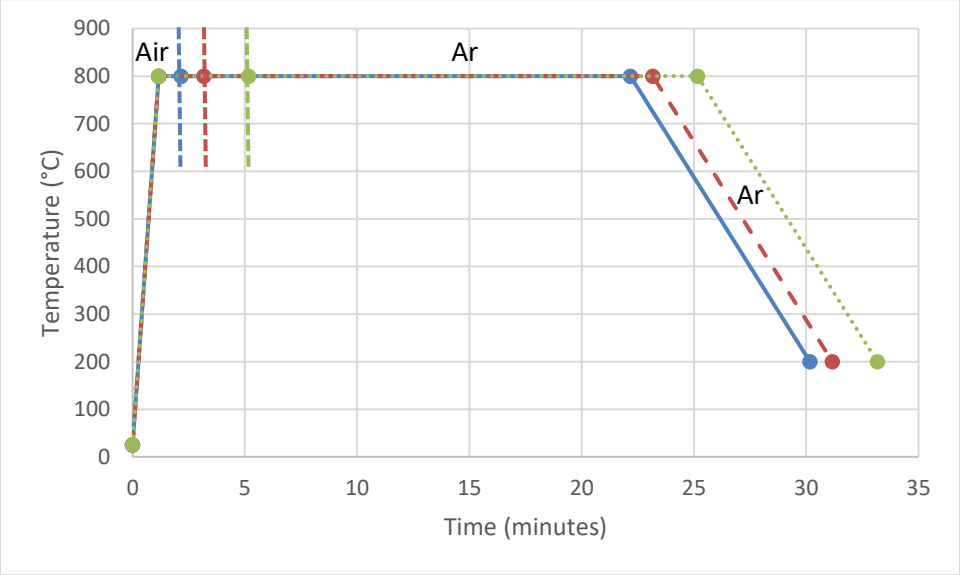


**Figure 2.5** Heat treatments for samples 10, 11, and 12. Samples placed in a pre-heated 800°C air environment for 1, 2, and 4 minutes (respectively), then for 20 minutes in argon.

### 2.2.5 Annealing Procedure 5

1. A sample is placed in a cold furnace with argon flowing and then heated to 800°C.

2. Sample undergoes **20-minute** heat treatment in argon.

3. Still flowing argon, the furnace is cooled to 200°C and the sample is removed (See Figure 2.6).

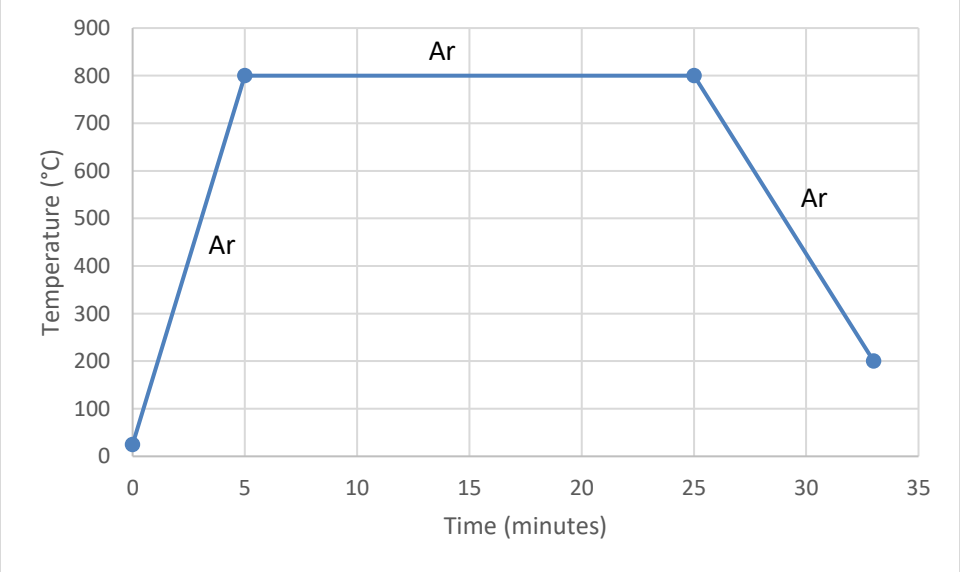


**Figure 2.6** Heat treatment for Sample 13. Sample placed in a room-temperature argon environment and brought to 800°C, then heat-treated for 20 minutes in argon.

### 2.2.6 Annealing Procedure 6

1. A sample is placed in a cold furnace with hydrogen flowing and then heated to 800°C.

2. Flow is changed from hydrogen to argon for a **20-minute** heat treatment.

3. Still flowing argon, the furnace is cooled to 200°C and the sample was removed (See Figure 2.7).

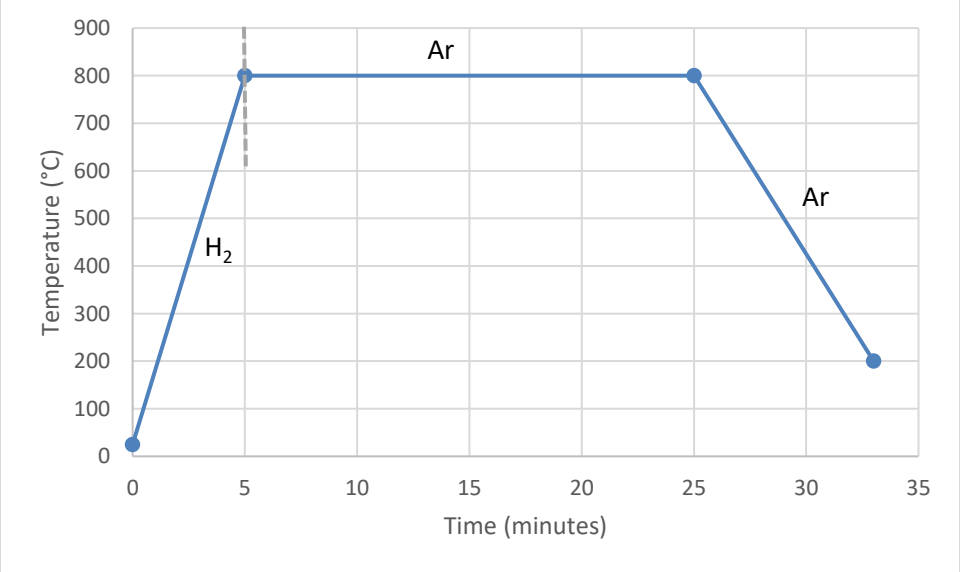


**Figure 2.7** Heat treatment for Sample 17. Sample placed in a room-temperature hydrogen environment and brought to 800°C, then heat-treated for 20 minutes in argon.

### 2.2.7 Growth Procedure 1

1. A sample is placed in a furnace preheated to 800°C while air is flowing for a 4-minute heat treatment.

2. Flow is changed from air to argon for an additional 20-minute heat treatment.

3. Sample is subjected to flowing argon and ethylene at 800°C for a 15-minute growth.

4. With ethylene turned off, but still flowing argon, the furnace is cooled to 200°C and the sample is removed (See Figure 2.8).

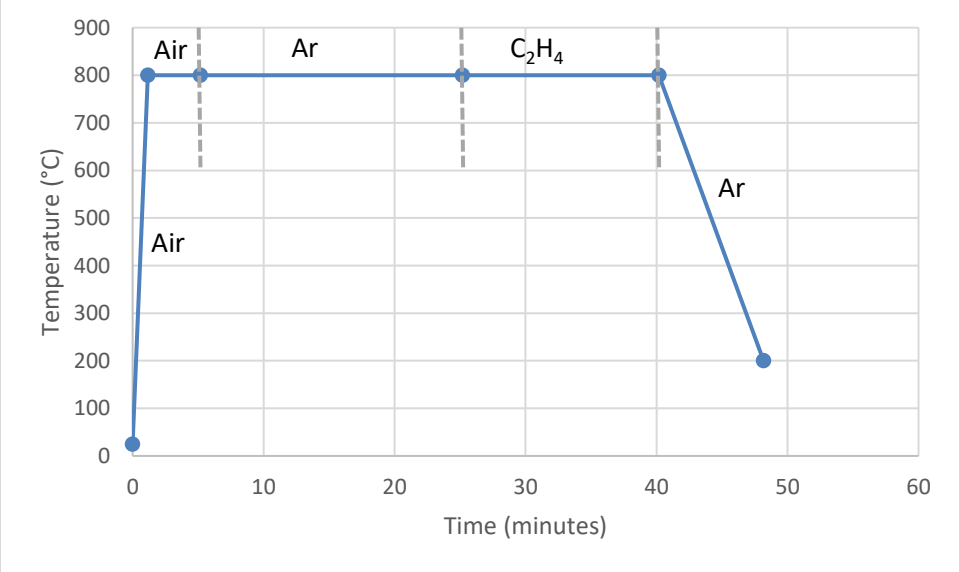


**Figure 2.8** Heat treatment for Sample 14. Sample placed in a pre-heated 800°C air environment for 4 minutes, then argon for 20 minutes, followed by ethylene for 15 minutes.

### 2.2.8 Growth Procedure 2

1. A sample is placed in a furnace preheated to 800°C while air is flowing for a 4-minute heat treatment.

2. Flow is changed to argon and ethylene for a 15-minute growth at 800°C.

3. With ethylene turned off, but still flowing argon, the furnace is cooled to 200°C and the sample is removed (See Figure 2.9).

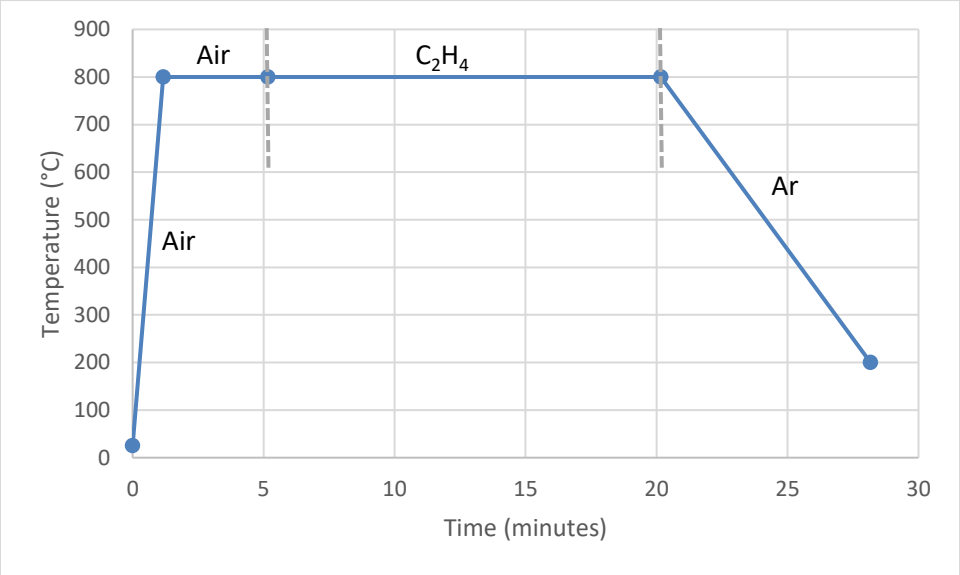


**Figure 2.9** Heat treatment for Sample 15. Sample placed in a pre-heated 800°C air environment for 4 minutes, then ethylene for 15 minutes.

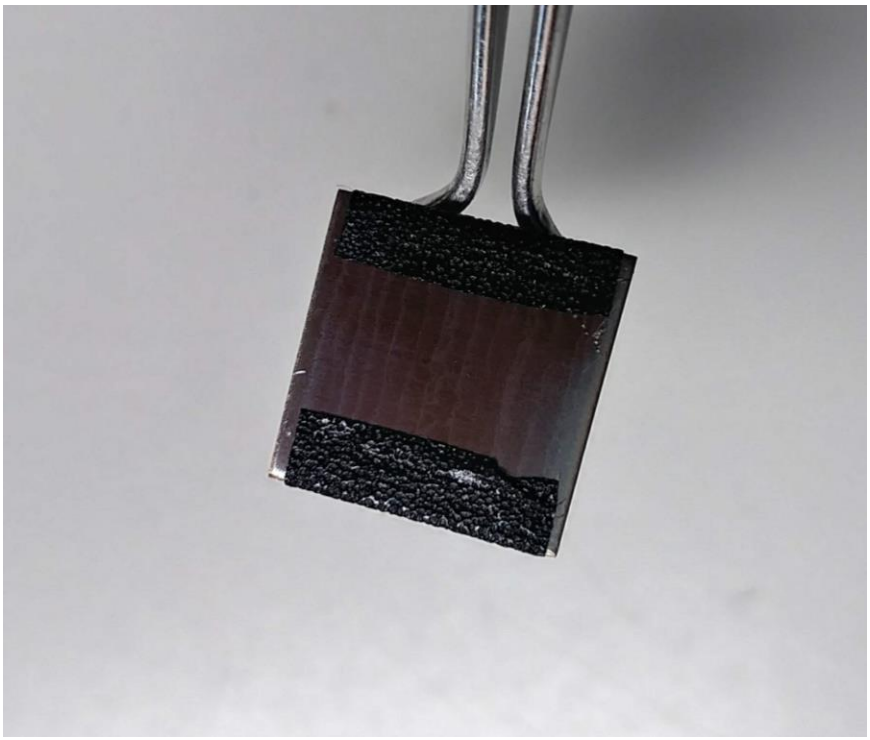

**Figure 2.10** A 1 cm x 1 cm stainless steel square after heat treatment in air/argon at 800°C (annealing procedure 2). Notice the 'browning' of the stainless-steel surface.

## 2.3 Analysis methods

### 2.3.1 SEM Imaging

After the first twelve samples mentioned in the previous section were attained, we imaged the surfaces using the Verios (SEM). This allowed us to compare surface characteristics to better ascertain the effect that different annealing times had on the material.

The samples were imaged using an accelerating voltage of 5 keV and a current of 10 nA with an Everhart-Thornly detector (ETD). Following are images of the surface of the twelve samples.

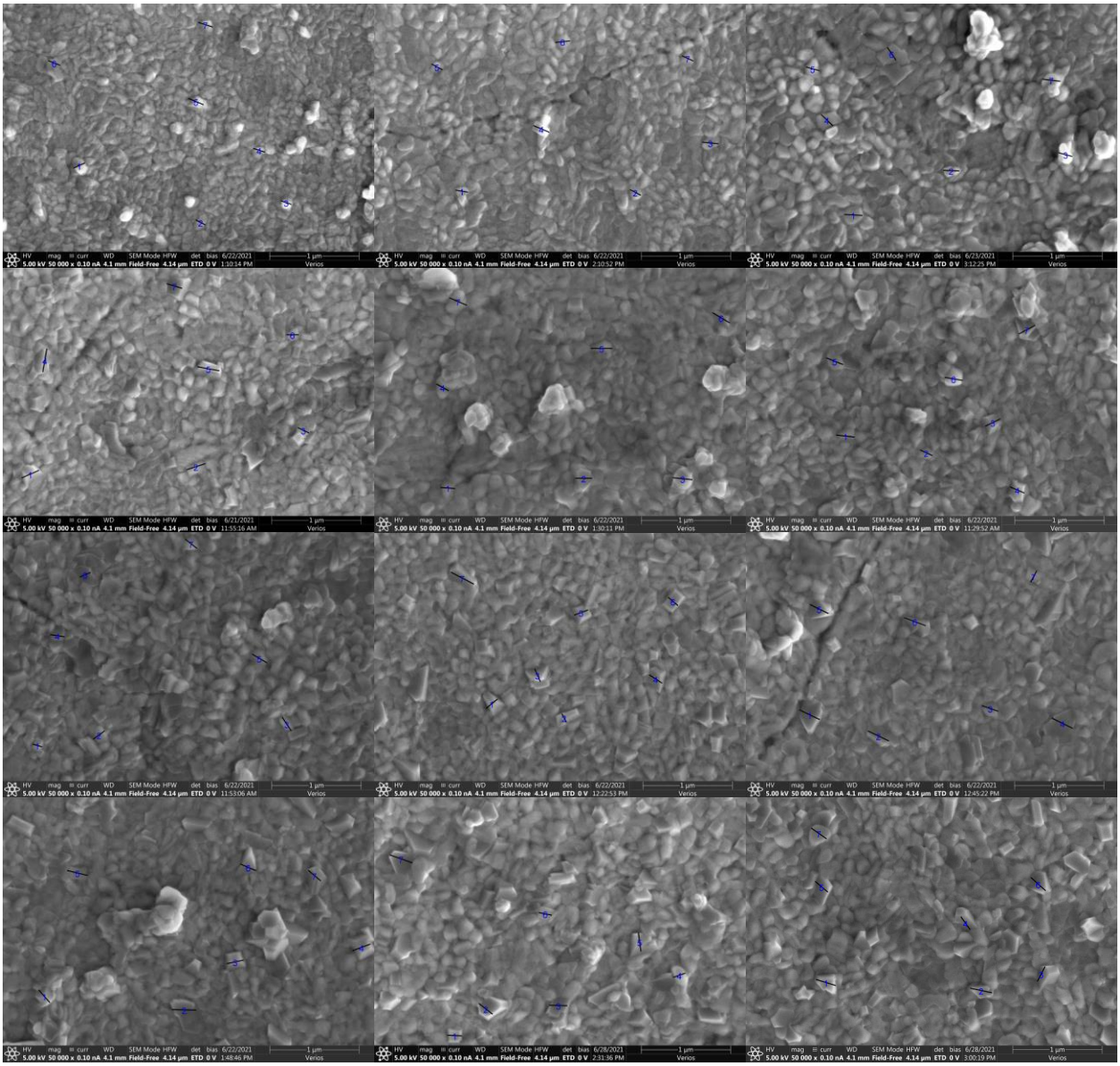

**Figure 2.11** Scanning Electron Micrographs (SEM) of samples 1-12: The columns represent 1, 2, and 4 minutes in air. The rows represent 0, 5, 10, and 20 minutes in argon. A constant temperature of 800°C was kept during the air and argon flows. The scale bar for all these images is 1µm. The top right-hand corner is Sample 3, and the bottom right-hand corner is Sample 12.

### 2.3.2 EDX Analysis

EDX analysis of samples 3 and 12 was conducted in the Verios. The purpose of EDX was to try to get an idea of the chemical composition of the surface, particularly the large crystal-like nodules, and to check if there was any observable change compared to the control.

Energy dispersive X-ray analysis was performed on various regions of the surface. Regions were chosen according to nodule characteristics. We tried to ascertain any difference in composition between large nodules observed on some grains and the less pronounced nodules found uniformly everywhere.

This was done at two different voltages and currents. For a larger area encompassing many nodules, a voltage of 15 keV with a current of 1.6 nA was used, while a voltage of 3.5 keV and current of 3.2 nA was used on scans localized on individual nodules.

### 2.3.3 FIB Sample Prep for TEM

After analyzing the sample surfaces with EDX, the next step is to do a cross-sectional EDX with TEM to get a better picture of what is happening at the surface. The first step in this process is performing TEM sample prep using the focused ion beam (FIB) on the Helios SEM. Samples were prepared in the usual way. The basic procedure is as follows:

1. At eucentric height, the stage is tilted to be perpendicular to the ion beam. Both the ion and electron beams should be aligned and made coincident.
2. A 1-micron wide, 10-micron long, and half-micron thick layer of platinum is laid down on the surface to protect the surface from the ion beam.
3. Using the ion beam, two trenches are milled in the surface, creating a small bridge one micron thick, 8-10 microns wide, and two microns deep (see figure 2.12a).

4. Re-tilting the stage to level, a J-cut is made (see figure 2.12b).
5. The Omniprobe micromanipulator is inserted, welded to the lamella, and the J-cut is completed, separating the lamella from the larger sample.
6. The lamella is then lifted out, transferred, and fused to a TEM grid. The micromanipulator is separated and removed (see figure 2.13).
7. Using a series of cleaning cuts, the lamella is then carefully milled to less than 100 nm in thickness (see figure 2.14).

Figures 2.12-2.14 show different stages of the process.

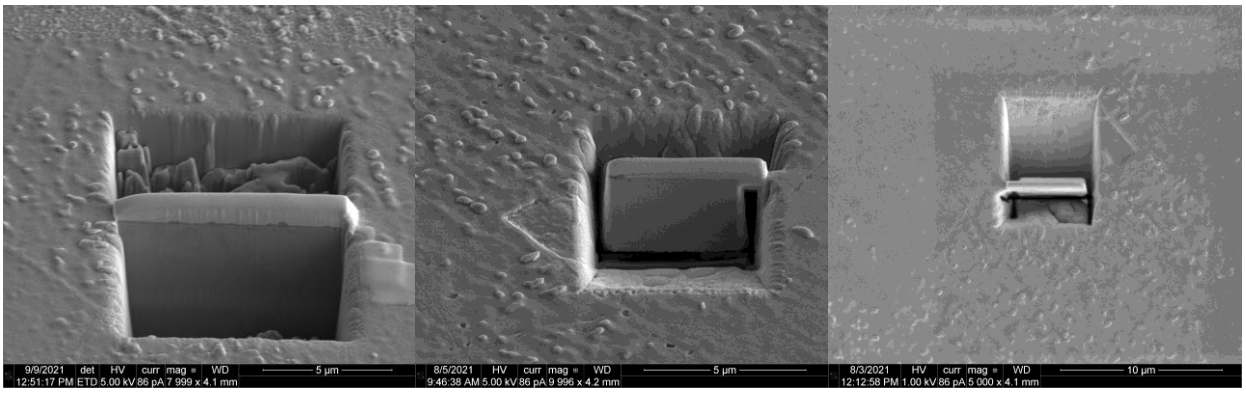


**Figure 2.12** SEM of samples 3 and 12, milled in preparation for lift out. The scale bar for the left two images is 5µm. The left is 10µm.

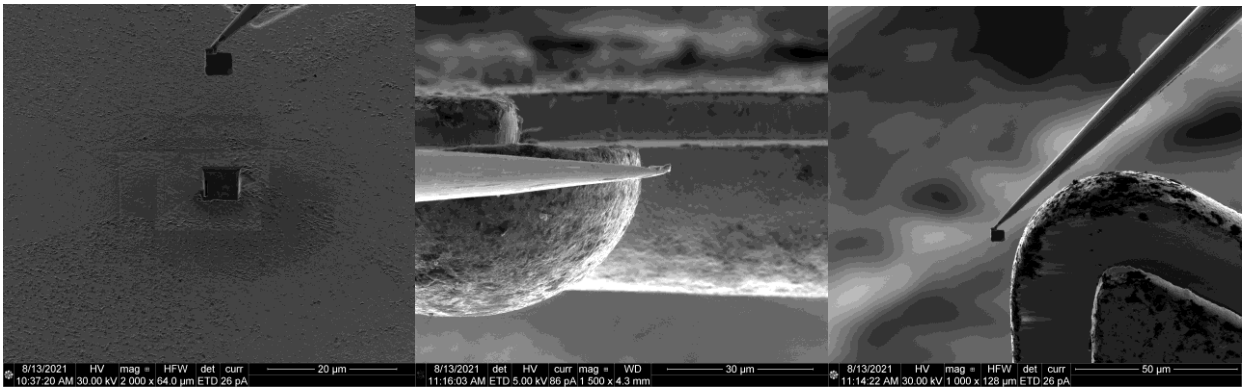


**Figure 2.13** SEM of lift out and insertion on TEM grid. The scale bars from left to right are 20, 30, and 50µm (respectively).

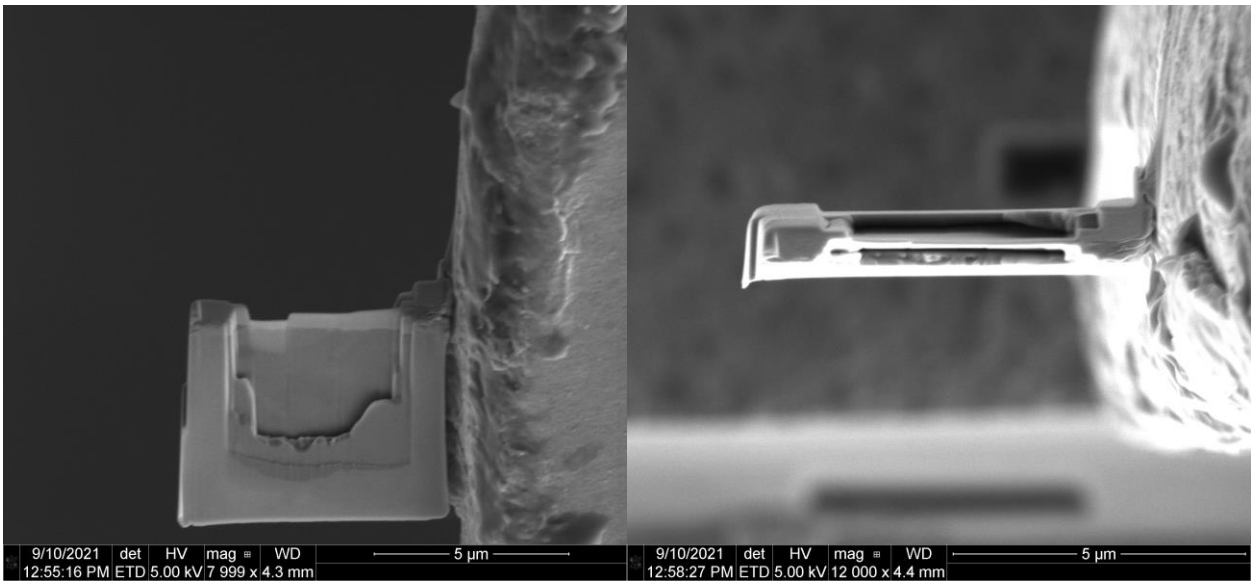


**Figure 2.14** SEM of Sample 12, thinned to 100 nm. The scale bars are 5µm.

### 2.3.4 TEM Imaging

The samples were then imaged and analyzed in the TEM. Paul Minson was indispensable in the acquiring of data in this step. Both TEM and STEM EDX were performed characterizing the substrate, surface, and regions at the base of carbon nanotube growth.

# 3 Results and Conclusions

This chapter covers the results and analyses by applying of the methods described in Ch. 2. Comparisons and other studies are then considered followed by concluding remarks and future work.

## 3.1 Results

It was found that there was nodule growth across the entire surface. The nodules grew with longer heating in air and became slightly more faceted with longer heating in argon. Nodule size did not change significantly throughout argon heating. It was based on these observations that we decided to do further analysis on samples 3 and 12.

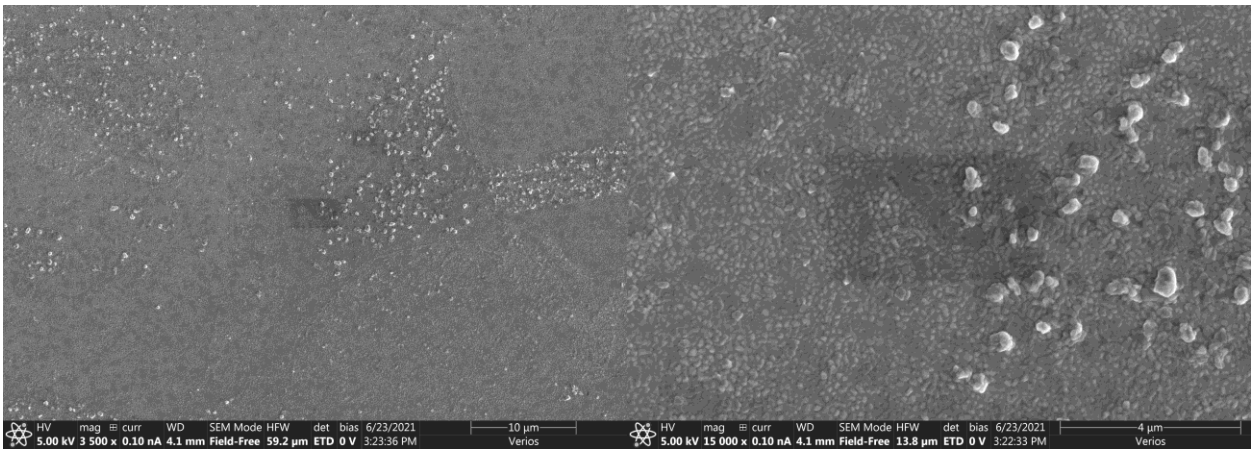


**Figure 3.1** SEM of Sample 3, 4 minutes in air at 800°C, showing grain structure and differences in nodule size between grains. The scale bars from left to right are 10, and 4µm (respectively).

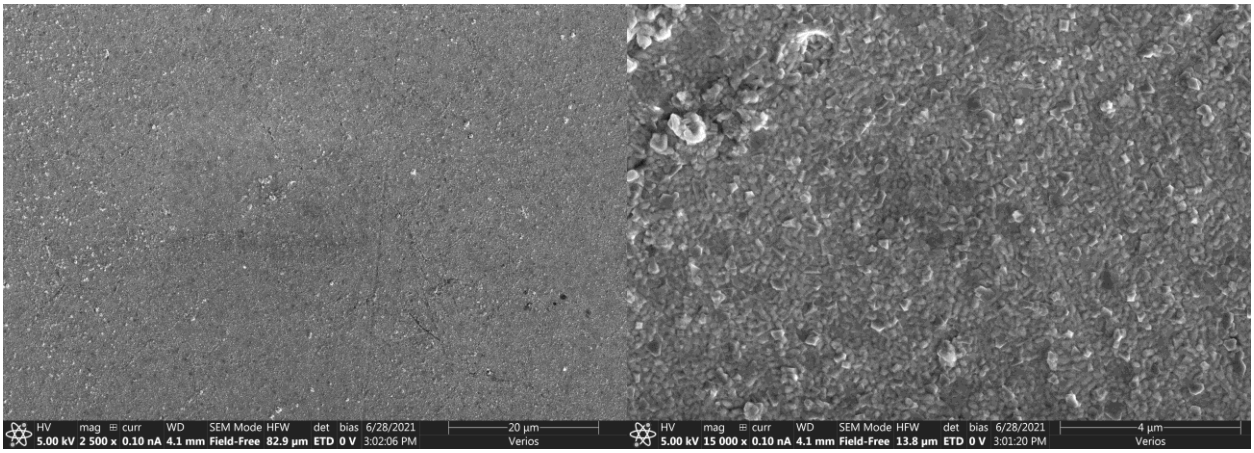


**Figure 3.2** SEM of Sample 12, 4 minutes in air and 20 minutes in argon at 800°C, showing grain structure and differences in nodule size between grains. The scale bars from left to right are 20, and 4µm (respectively).

These images show that there is little difference in the size of nodules between samples 3 and 12. Though, there is greater faceting seen in the images of Sample 12. The nodules average width is just under 200 nm as seen in Figures 3.3, 3.4 and Table 1 in the appendix. These samples are our baseline from which we will conduct our analysis.

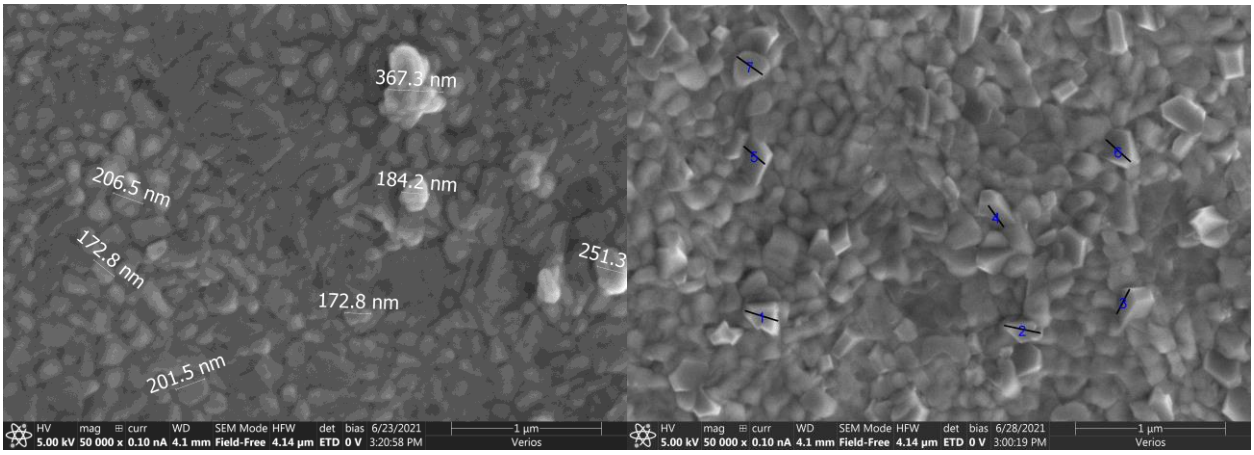


**Figure 3.3** SEM of Sample 3 (left) and Sample 12 (right), showing actual and relative sizes of nodules. The scale bars are 1µm.

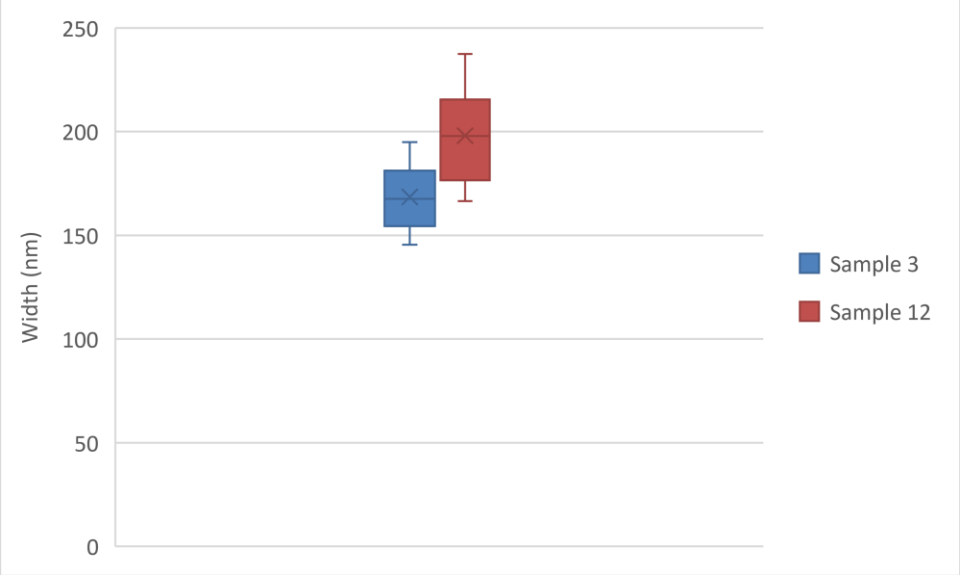


**Figure 3.4** Nodule sizes (nm) of Sample 3 and Sample 12 (max, min, mean, median, and quartiles).

Figure 3.5 shows regions on samples 3 and 12 where EDX analysis was done. There is evident variation in grain structure and large nodule concentration across grain boundaries. Also of interest are darker areas from which it appears material has migrated away. The lighter regions are the larger nodules, and the darker regions are the holes left behind after diffusion.

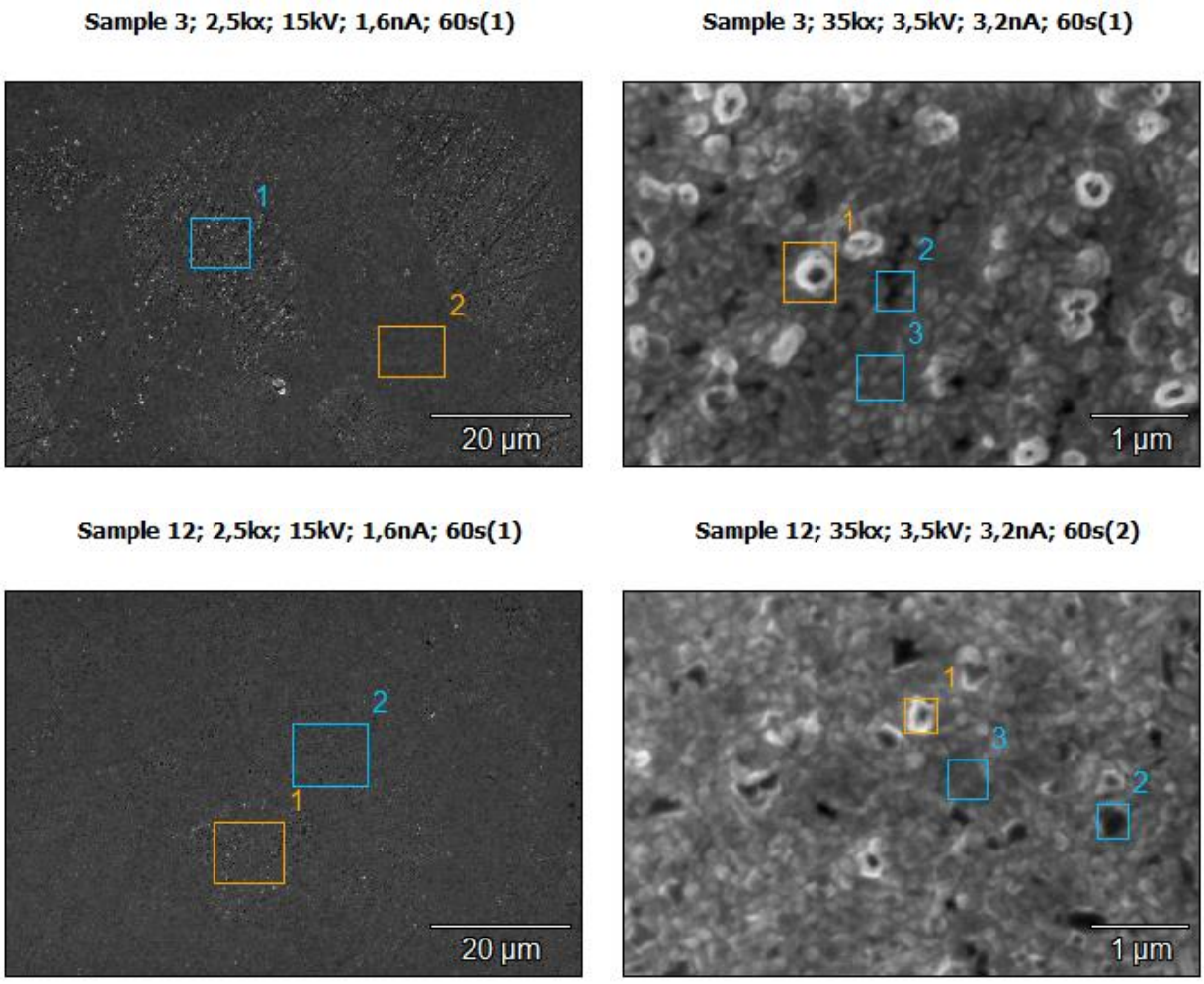


**Figure 3.5** SEM of Samples 3 and 12 at 2.5kx and 35kx magnification.

### 3.1.1 Sample 3

Figure 3.6 shows the EDX spectra from two regions of Sample 3 overlayed on an EDX spectrum taken from a control sample. These three spectra were normalized to the Fe Kα line. Region 1 shows higher Cr counts than the control, as well as an apparent higher density/size of surface nodules. In contrast, region 2 shows lower Cr counts.

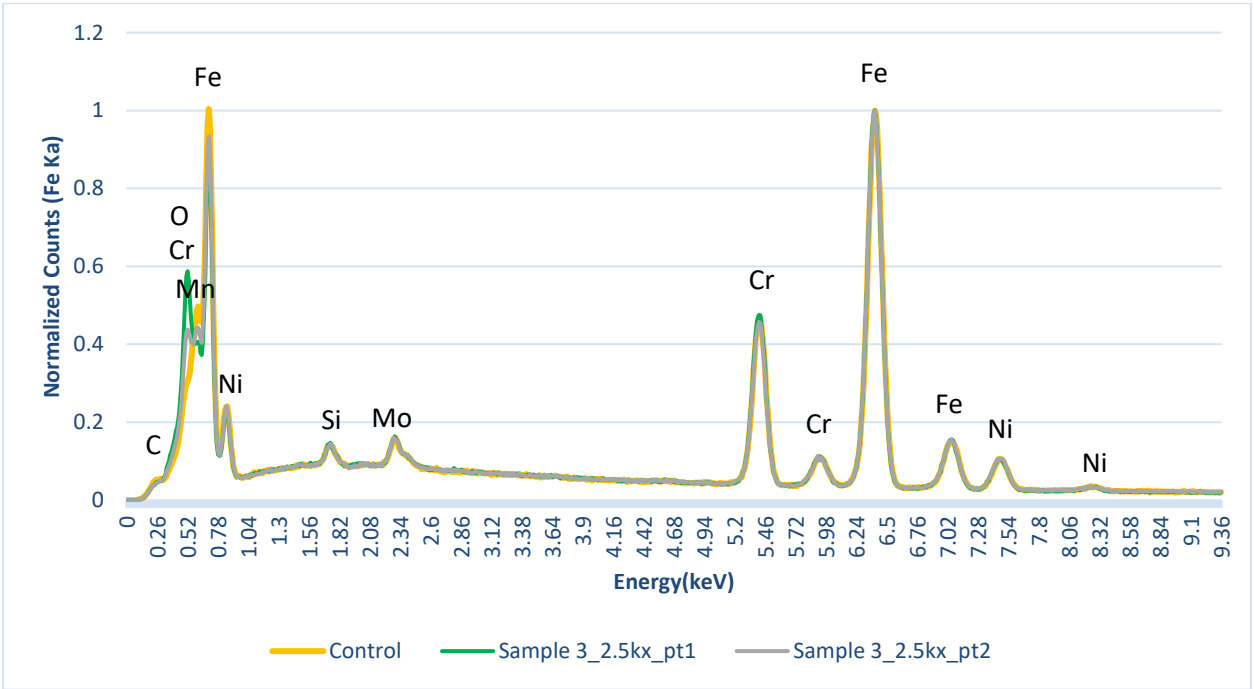


**Figure 3.6** EDX of Sample 3 regions shown in SEM (top); at 2.5kx, 15keV, 1.6nA, for 60s.

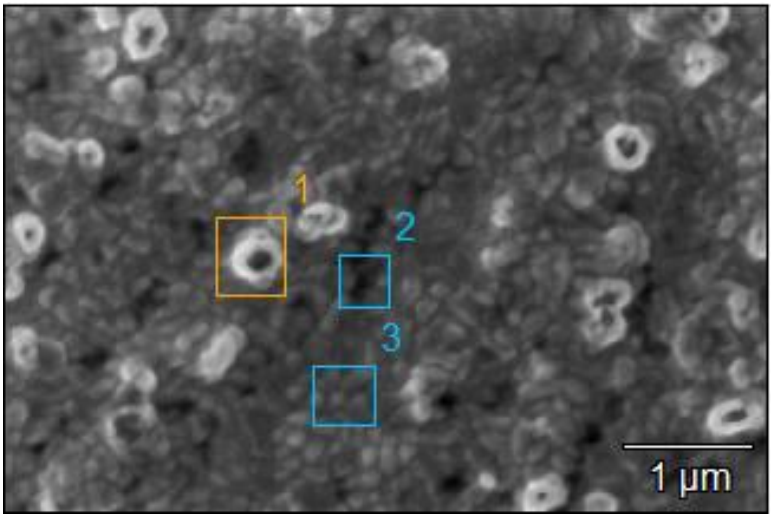


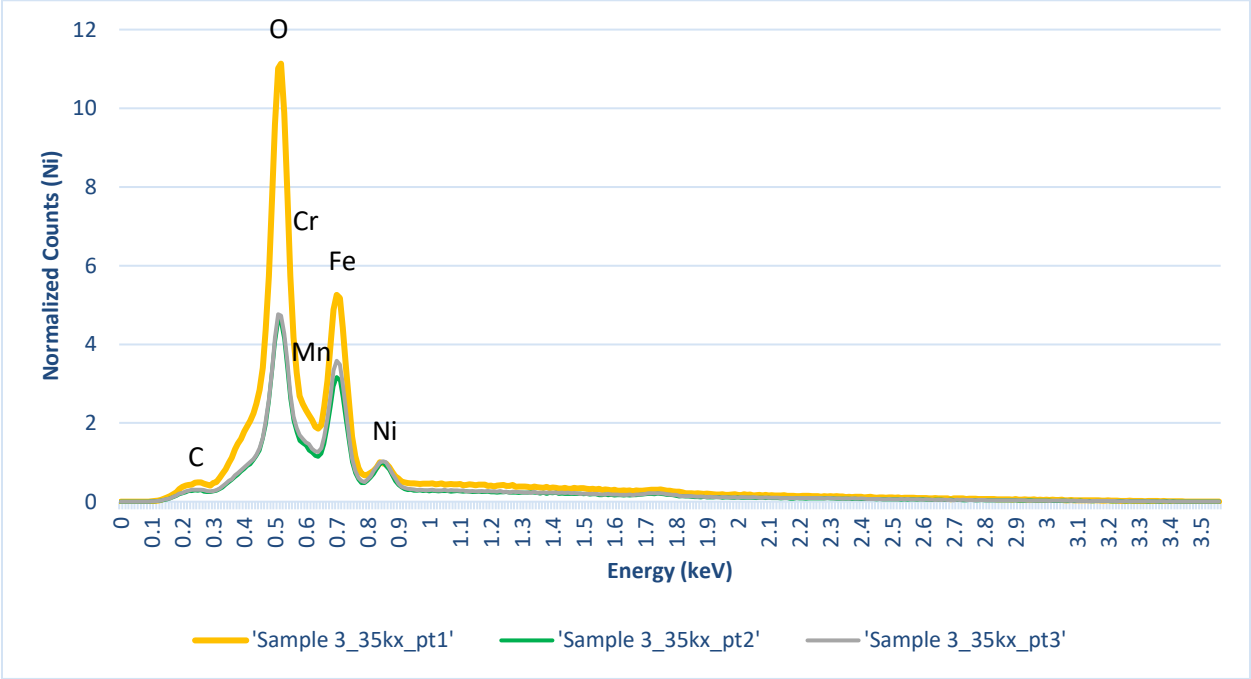


**Figure 3.7** EDX of Sample 3 regions shown in SEM (top); at 35kx, 3.5keV, 3.2nA, for 60s.

Likewise, individual surface nodules from Sample 3 show a definite increase in the relative abundance of oxygen and chromium compared to the iron and nickel. This seems to suggest that the nodules are chromium oxides.

### 3.1.2 Sample 12

A similar pattern is found when we look at spectra from different regions of Sample 12. Though, regions of large nodule growth have more similar concentrations of chromium and iron than regions with small nodule growth.

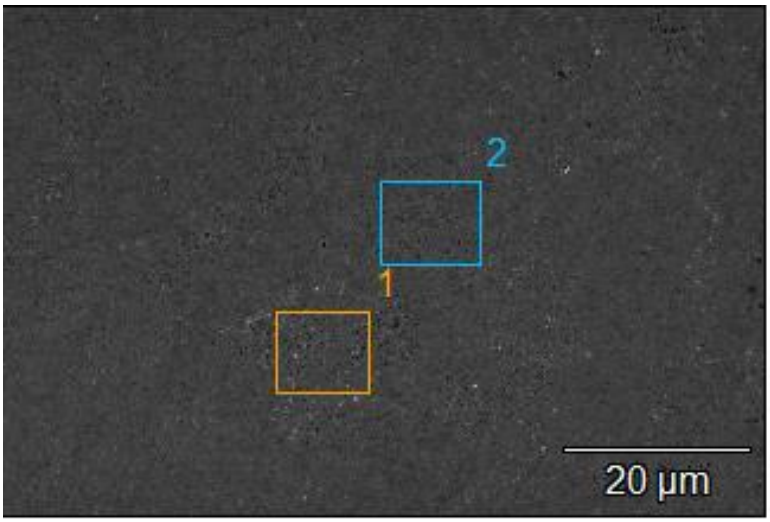


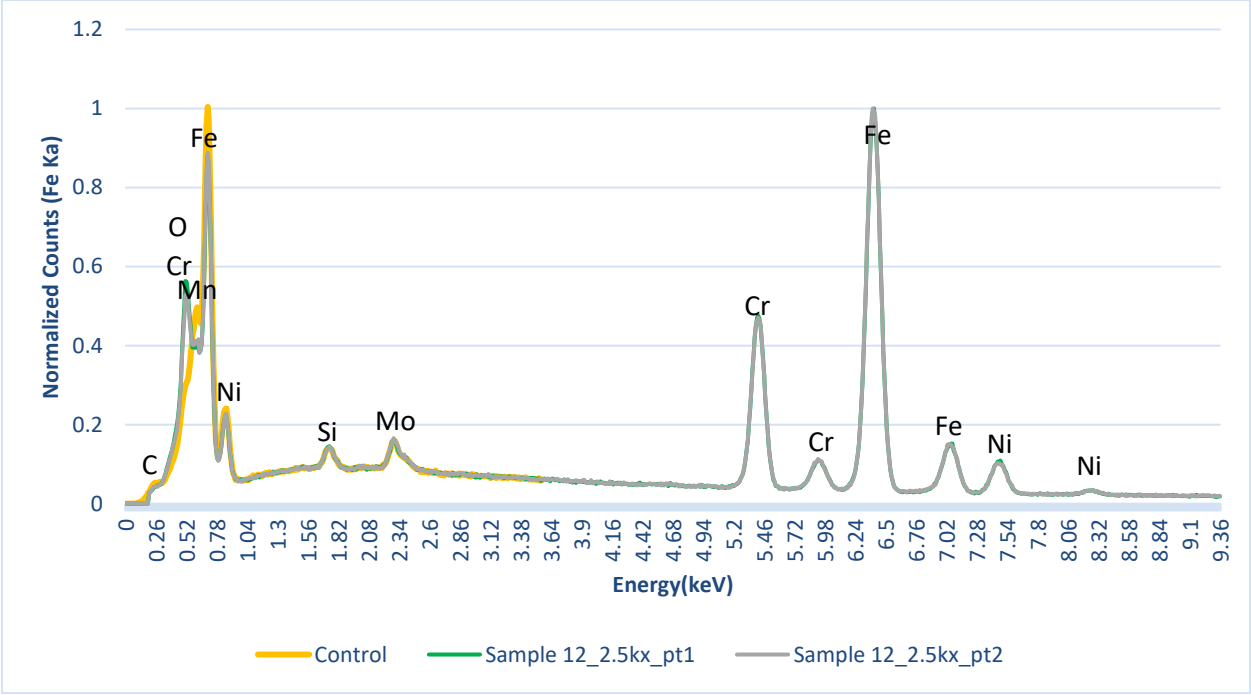


**Figure 3.8** EDX of Sample 12 regions shown in SEM (top); at 2.5kx, 15keV, 1.6nA, for 60s.

Additionally, when examining an individual nodule, we find a definite increase in the relative abundance of oxygen and chromium compared to the iron and nickel. This again supports the idea that the nodules are chromium oxides.

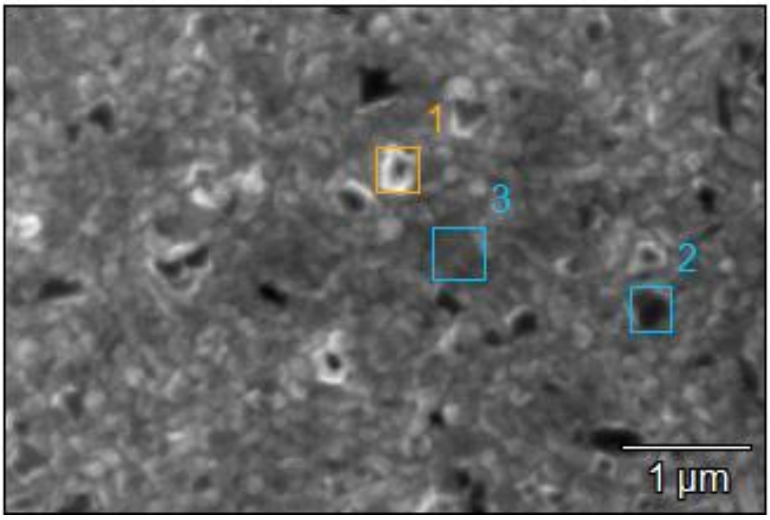


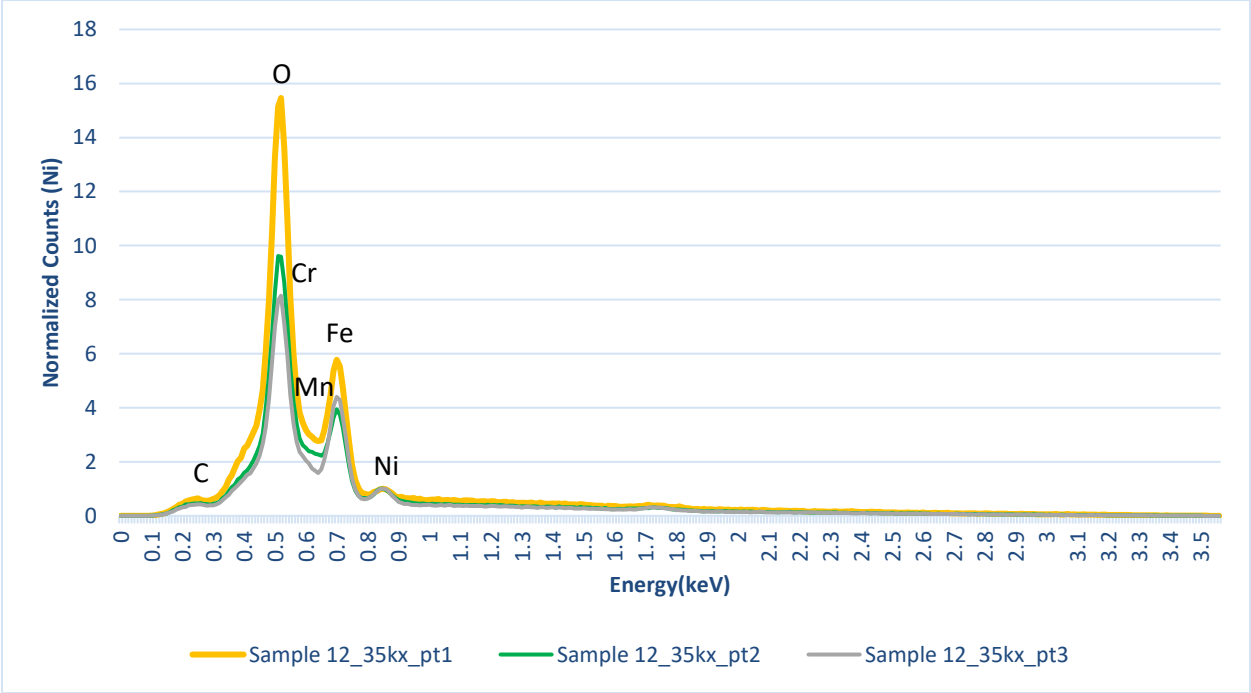


**Figure 3.9** EDX of Sample 12 regions shown in SEM (top); at 35kx, 3.5keV, 3.2nA, for 60s.

### 3.1.3 Sample 13

Sample 13 was prepared to examine if the oxygen in the air during heat treatment affected the nodule growth. The sample was heated for 20 minutes in argon only. The sample still shows nodule growth like in the previous samples. To verify, EDX was done on this sample as well.

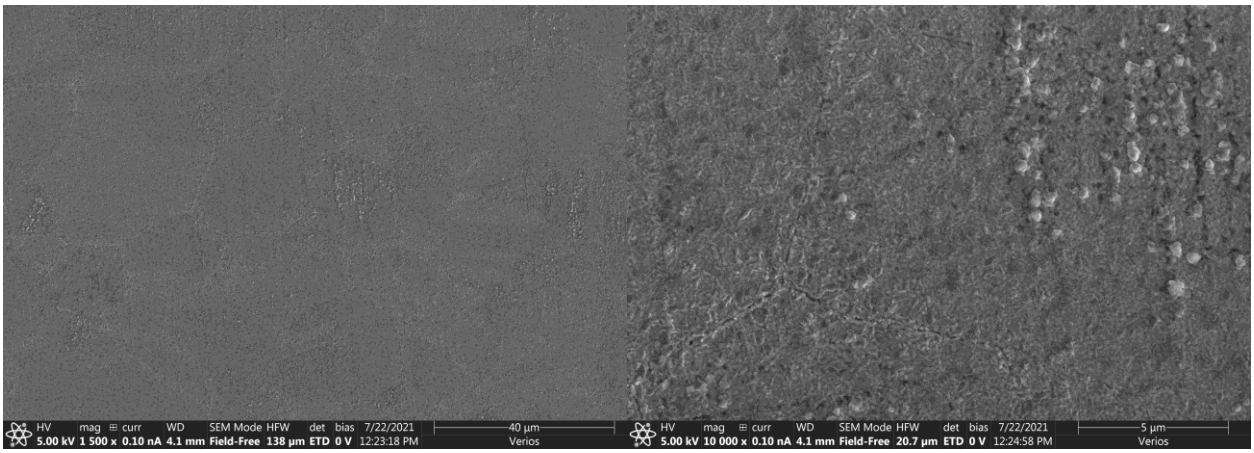


**Figure 3.10** SEM of Sample 13: 1.5kx (left) and 10kx (right) magnifications of Sample 13, 20 minutes in argon at 800°C, showing grain structure and differences in nodule size between grains. The scale bars from left to right are 40, and 5µm (respectively).

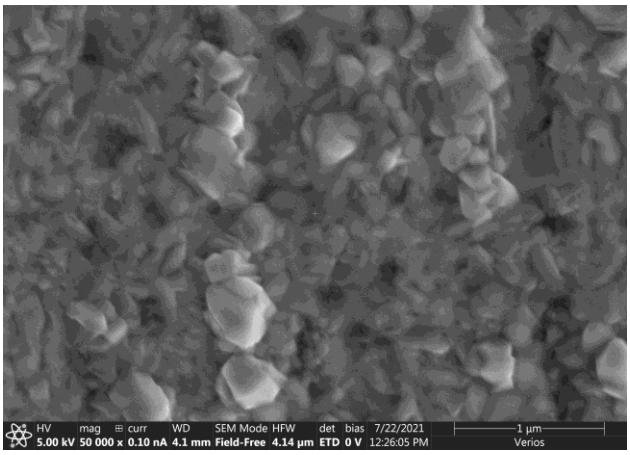


**Figure 3.11** SEM of Sample 13 at 50kx magnification. The scale bar is 1µm.

It was found that the nodule structure and composition are like those in samples 3 and 12. Because the proximity of the O and Cr peaks makes it difficult to ascertain which chemical abundance is changing the most, TEM analysis is needed.

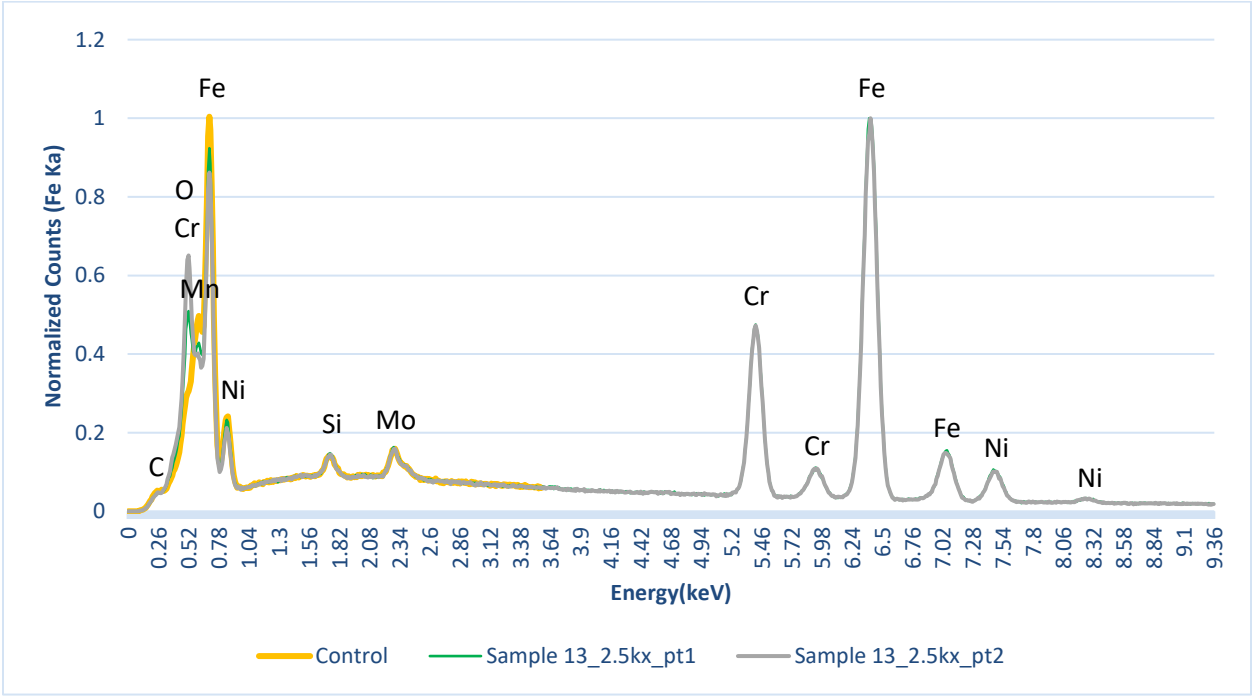


**Figure 3.12** EDX of Sample 13 regions shown in SEM (top); at 2.5kx, 15keV, 1.6nA, for 60s.

Additionally, individual nodules appear to have a similar composition to those in the other samples. It does not appear that there is a significant difference between heat treatment in air followed by argon, versus a heat treatment only in argon.

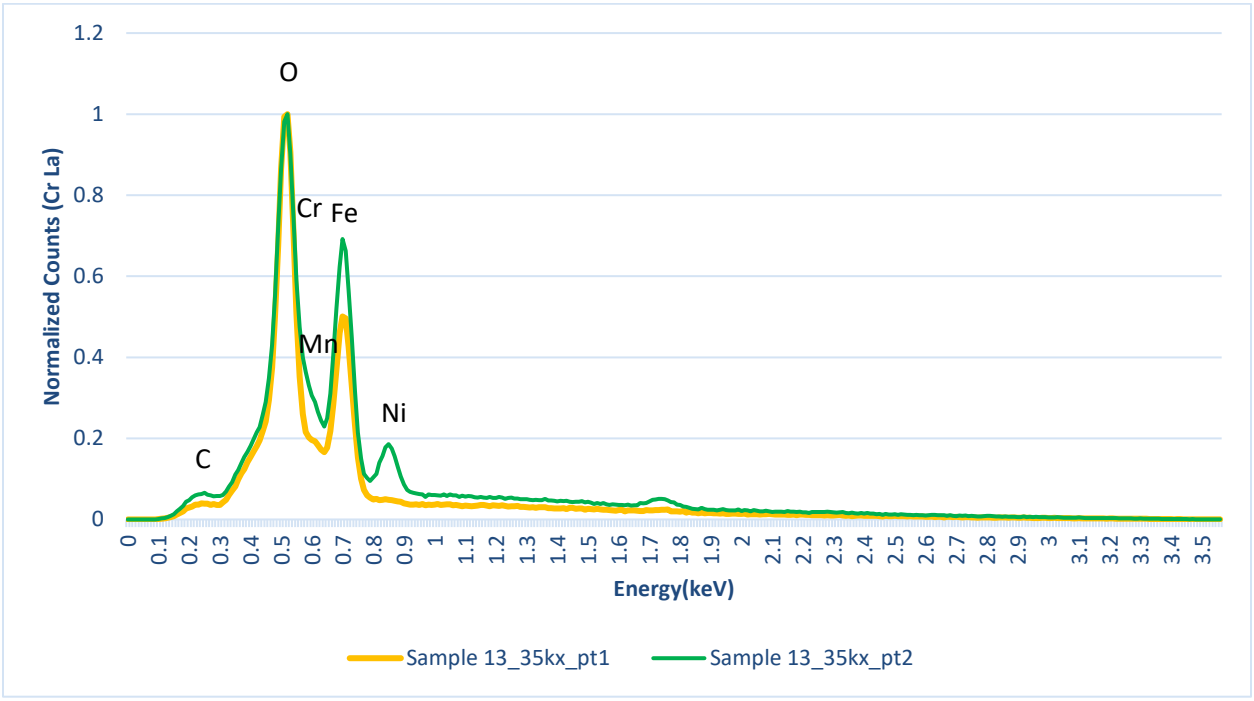


**Figure 3.13** EDX of Sample 13 regions shown in SEM (top); at 35kx, 3.5keV, 3.2nA, for 60s.

### 3.1.4 Sample 17

Sample 17 was prepared because it appeared from the analysis of Sample 13 that oxygen was still present and forming nodules with the chromium on the surface. For this experiment, the intent was to reduce the oxygen before heat treatment.

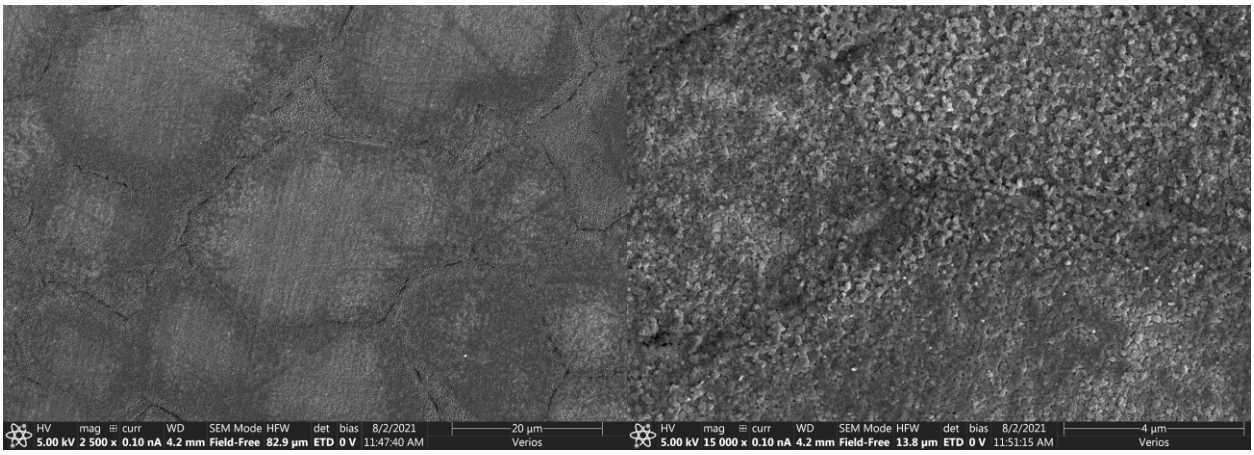


**Figure 3.14** SEM of Sample 17: 2.5kx (left) and 15kx (right) magnifications of Sample 17, reduction in $H_2$ before 20 minutes in argon at 800°C, showing grain structure and differences in nodule size between grains. The scale bars from left to right are 20, and 4µm (respectively).

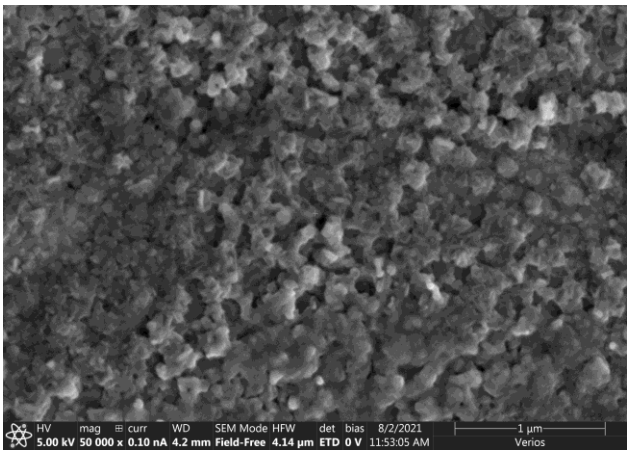


**Figure 3.15** SEM of Sample 17 grain boundary at 50kx magnification. The scale bar is 1µm.

The sample was exposed to a hydrogen atmosphere while the furnace was coming up to temperature. Once it was at 800°C, the atmosphere was changed to argon and heated for 20 minutes. The sample still showed nodule growth, but it is more concentrated around grain boundaries. To verify, EDX was done on this sample as well.

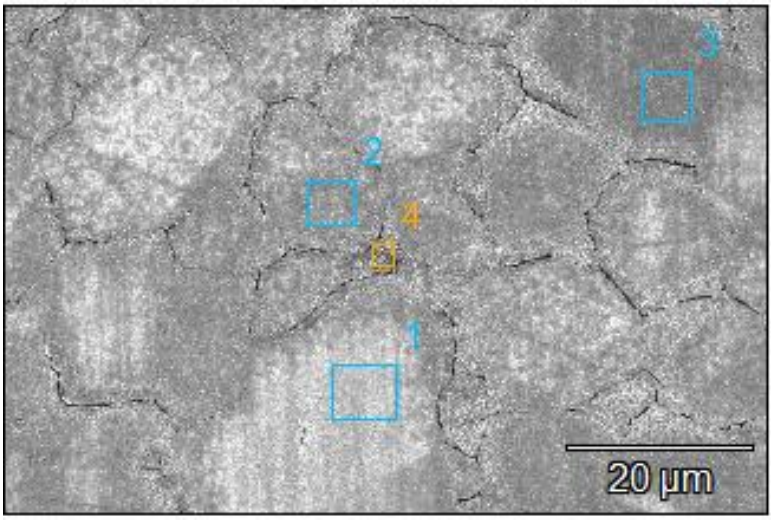


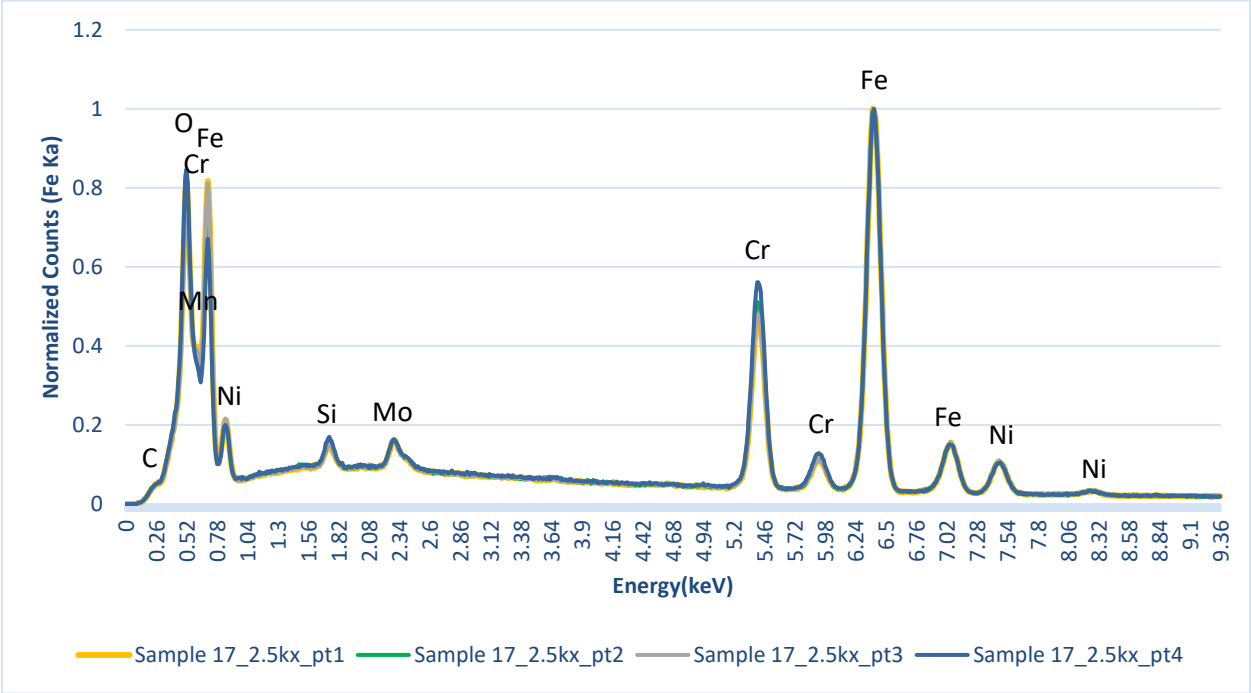


**Figure 3.16** EDX of Sample 17 regions shown in SEM (top); at 2.5kx, 15keV, 1.6nA, for 60s.

Interestingly, it appears that the relative abundance of iron has gone down, while chromium and oxygen appear to be more abundant. This is the opposite of what was intended. The reason for the difference is uncertain.

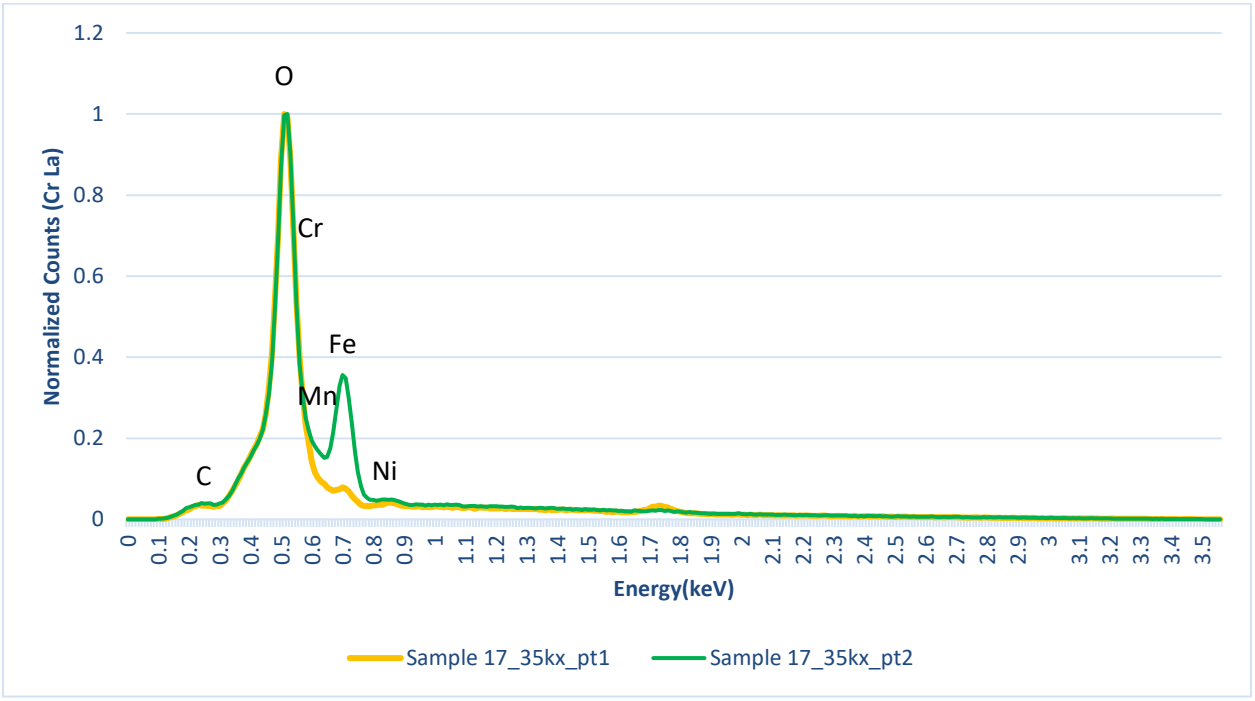


**Figure 3.17** EDX of Sample 17 regions shown in SEM (top); at 35kx, 3.5keV, 3.2nA, for 60s.

### 3.1.5 Samples 14 and 15

Samples 14 and 15 received the same annealing recipe as samples 12 and 3 (respectively), with additional processing for CNT growth. Sample 14 underwent a 4-minute heat treatment in air, followed by 20 minutes in argon and 15 minutes in ethylene. Sample 15 underwent 4 minutes in air followed by 15 in ethylene. Both show uniform but non-aligned CNT growth. SEM EDX was done on the samples, but little can be gleaned with SEM given the nanotube growth covering the surface.

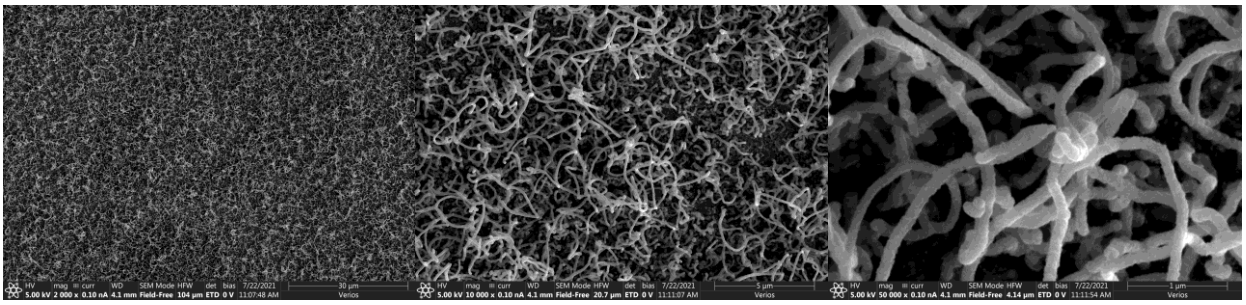

**Figure 3.18** SEM of Sample 14 at 2kx (left), 10kx (center), and 50kx (right) magnification. Scale bars are 30, 5, and 1µm (respectively).

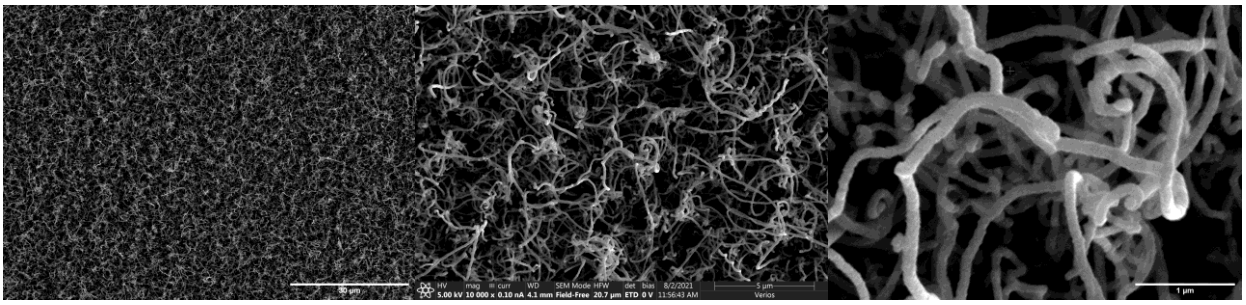

**Figure 3.19** SEM of Sample 15 at 2kx (left), 10kx (center), and 50kx (right) magnification. Scale bars are 30, 5, and 1µm (respectively).

## 3.2 S/TEM Analysis

EDX using SEM, while valuable for getting a broad characterization of the surface, was inconclusive as to the composition of individual nodules and the nature of regions at the base of carbon nanotubes. For this reason, the Control, and Samples 3, 12, and 15 were then analyzed using TEM and STEM. This gave us a higher resolution look at the regions in question.

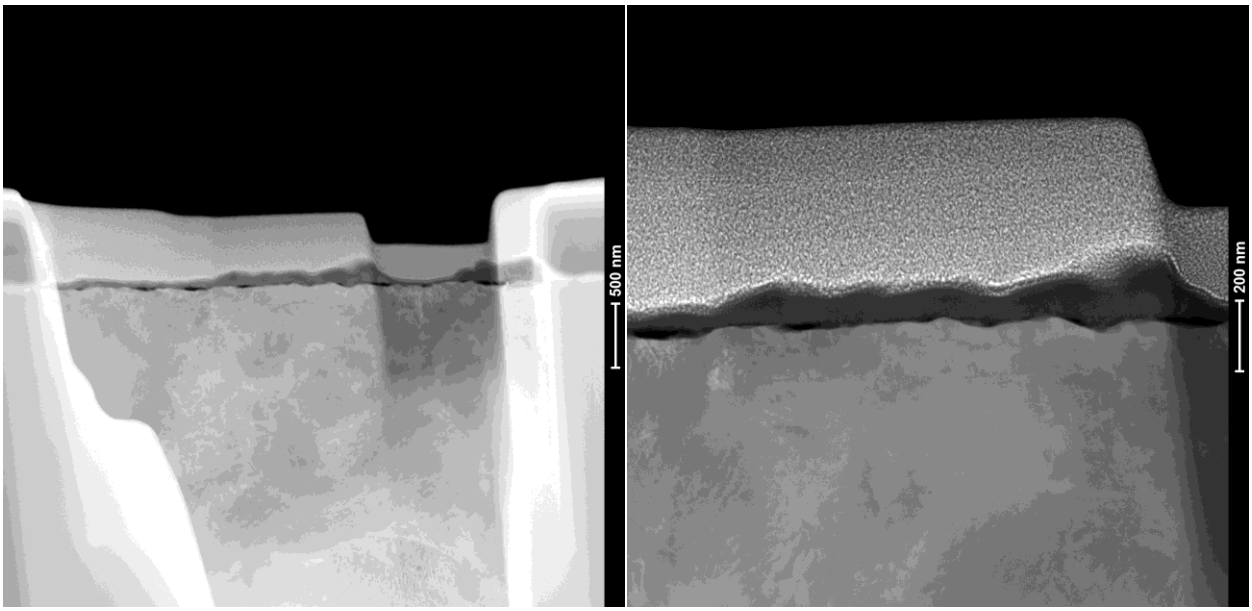


**Figure 3.20** Scanning Transmission Electron Micrograph (STEM) of Sample 12. The scale bars from left to right are 500, and 200 nm (respectively).

Figure 3.20 shows the cross section of the top surface layer, subsurface features, and substrate of Sample 12. The substrate is lighter, with apparent grain boundaries, and the dark region is the nodule covered surface. Analysis of the individual regions shows that the chemical signature is that of 316L, the substrate.

Figures 3.21-3.24 show various stages of TEM prep for the control and samples 3 and 15.

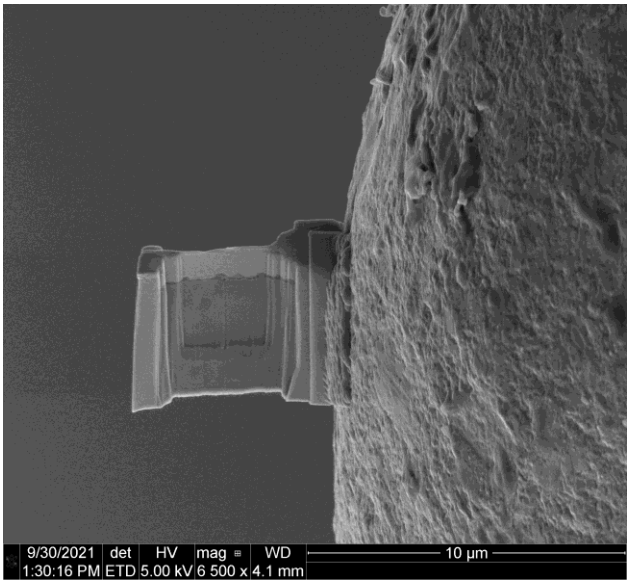


**Figure 3.21** SEM of Sample 3, thinned to 100 nm.

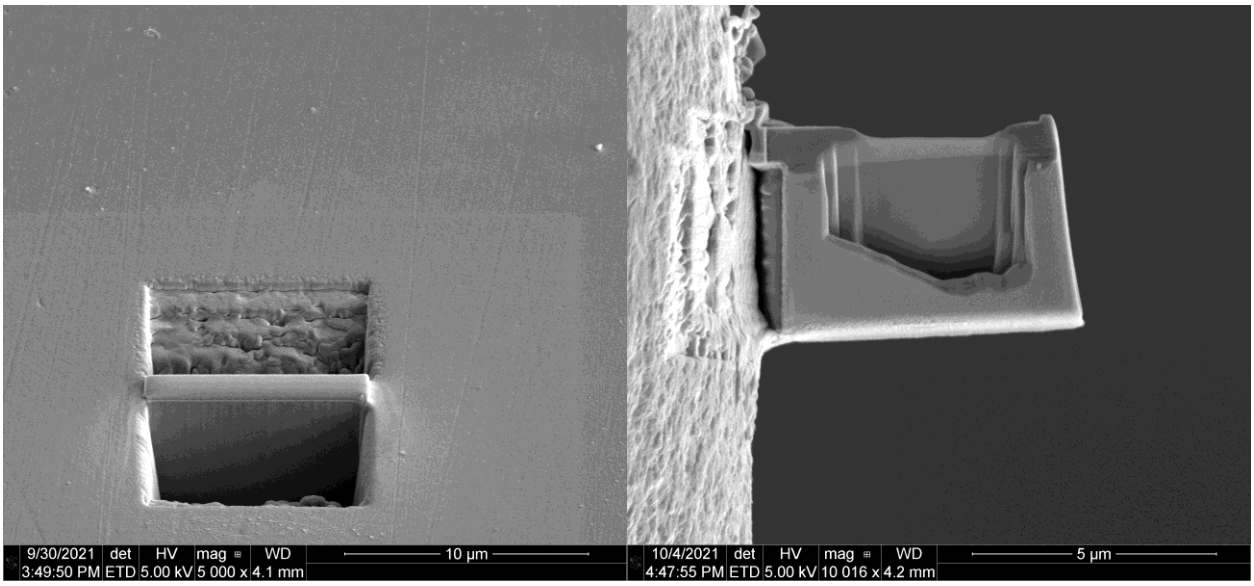


**Figure 3.22** SEM of control sample, thinned to 100 nm.

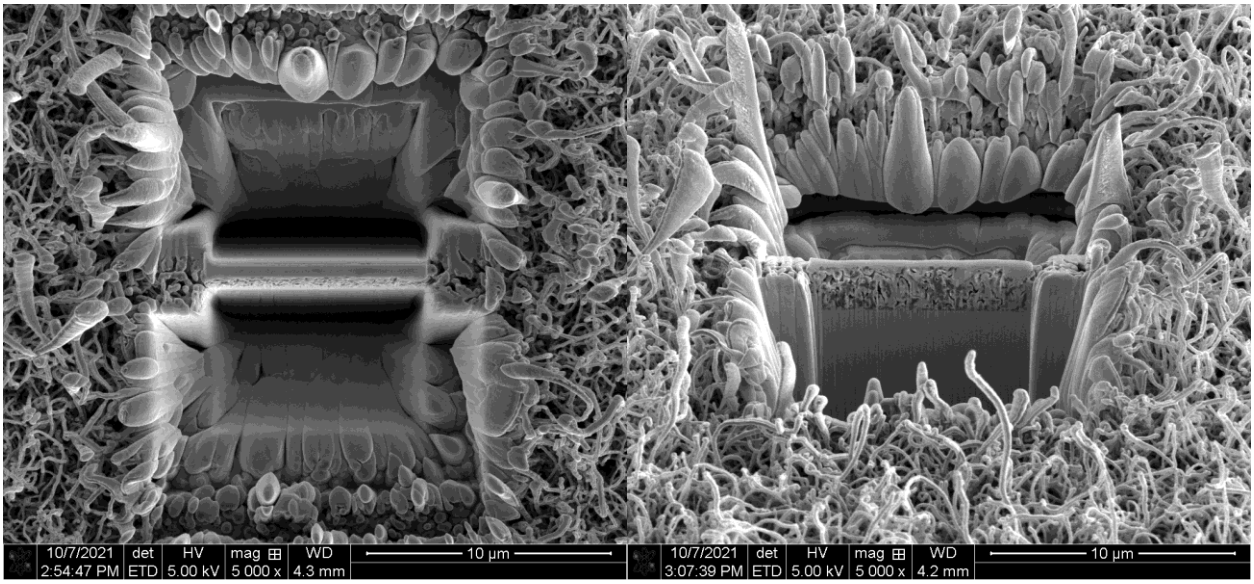


**Figure 3.23** SEM of Sample 15 TEM preparation.

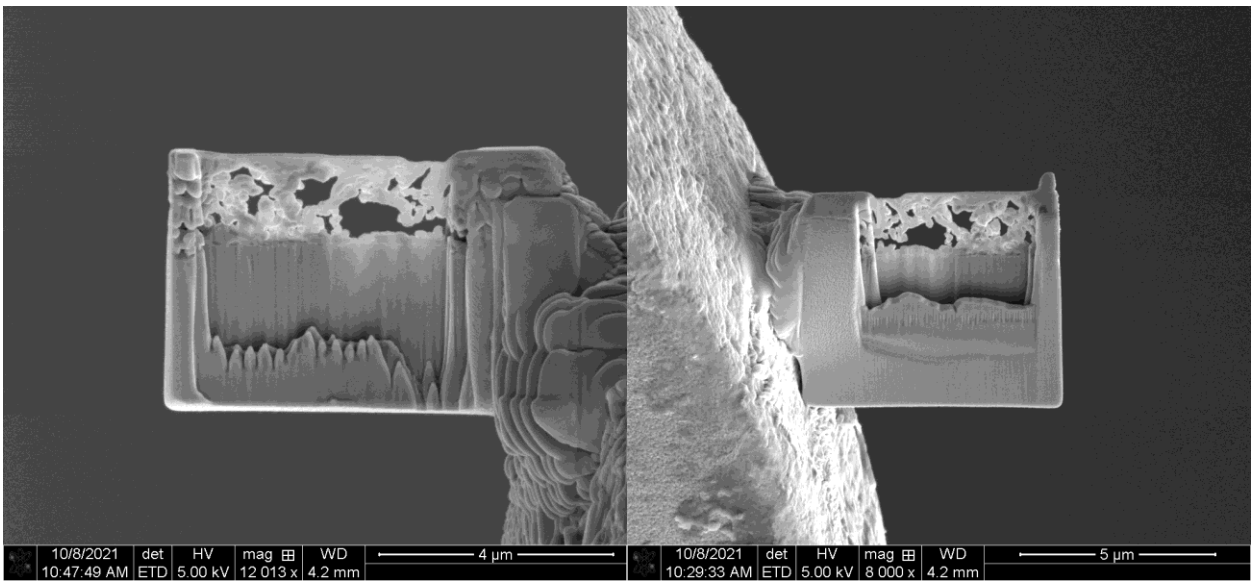


**Figure 3.24** SEM of Sample 15, thinned to 100 nm.

With TEM we can analyze the composition of each layer in the material. We define three separate regions: the substrate, subsurface, and surface. The substrate is the 316L stainless-steel unexposed to atmosphere. The subsurface is the region just below the surface showing similar properties to the substrate but with an apparent boundary separating it from the substrate. The surface is composed of the grown surface nodules observed in the SEM.

### 3.2.1 Sample 12 STEM

A typical spectrum of Sample 12 with common element peaks is illustrated in Figure 3.25. These peaks vary in amplitude as we move from the substrate to the surface of the sample.

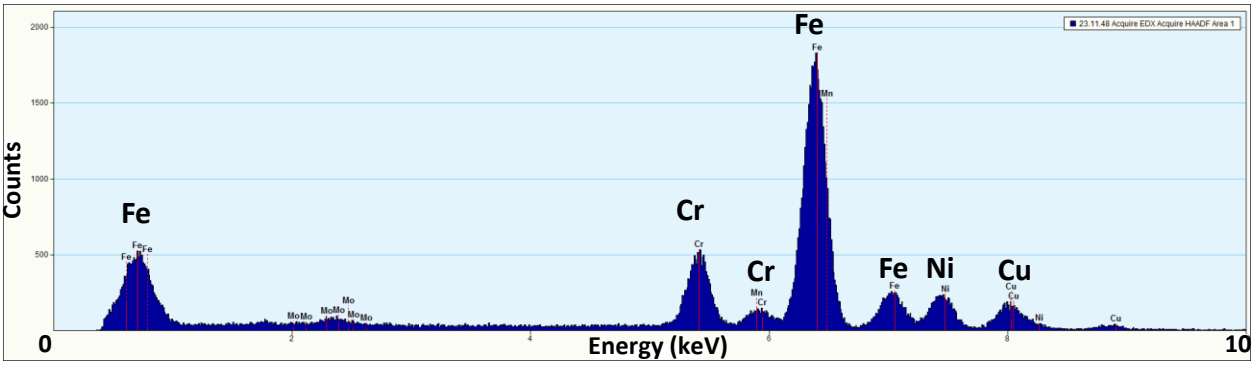


**Figure 3.25** EDX Spectrum of Sample 12 substrate showing baseline composition of 316L stainless steel. The labeled peaks are the elements of interest. The spectra in this section are all scaled to the same energy range (0-10 keV) in the horizontal axis for easy reference and comparison.

The spectra in Figure 3.26 are consistent with 316L stainless steel, with slight deviation of the chromium as we near the surface. The two regions were chosen based on a very slight apparent boundary between the two. No significant difference exists in the spectra.

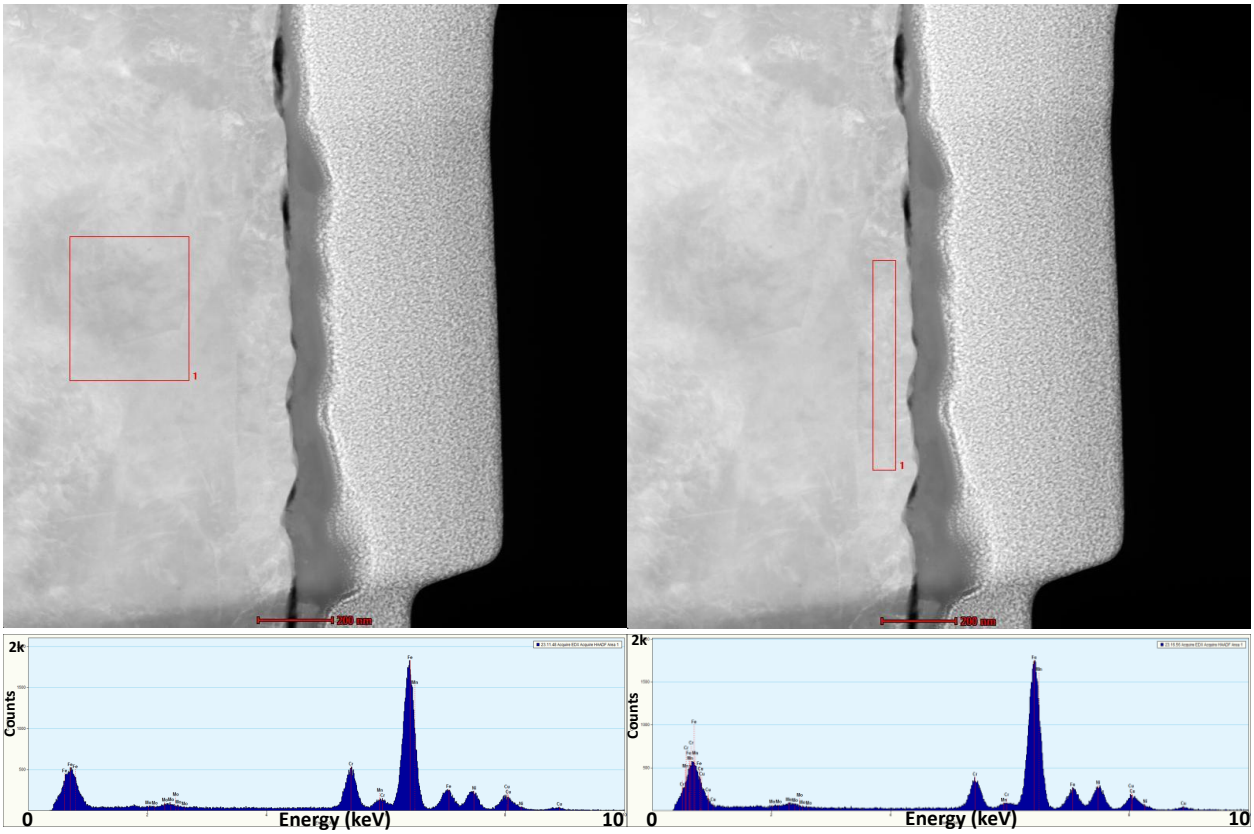


**Figure 3.26** STEM of Sample 12 substrate (left), subsurface (right) with EDX spectral signature. Energy ranges are 0-10 keV on horizontal axis.

In Figure 3.27 two regions within the surface nodules are displayed. The chromium and oxygen counts appear to have increased significantly, corroborated by the dark shade indicative of low Z material. Interestingly, the spectra of the dark surface layer are noticeably lacking any nickel. The speckled lighter area above the surface layer is the protective deposited platinum described in section 2.3.3.

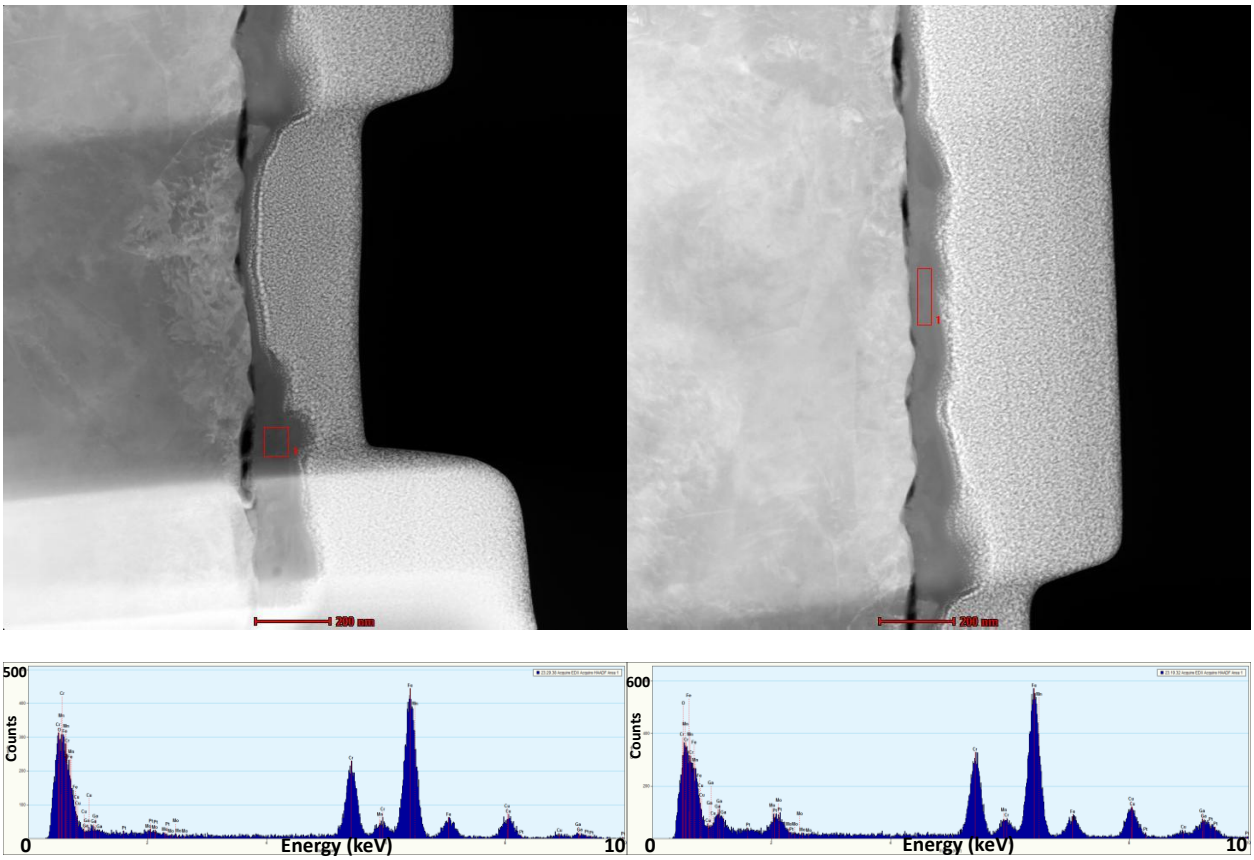


**Figure 3.27** STEM of Sample 12 large nodule (left), small nodule (right) with EDX spectral signature showing absence of nickel. Energy ranges are 0-10 keV on horizontal axis.

### 3.2.2 Sample 3 STEM

Sample 3 shows a similar spectral signature to Sample 12. The same reduction in chromium just below the surface can be seen (Figure 3.28), followed by an increase in chromium and disappearance of nickel in the surface layer (Figure 3.29).

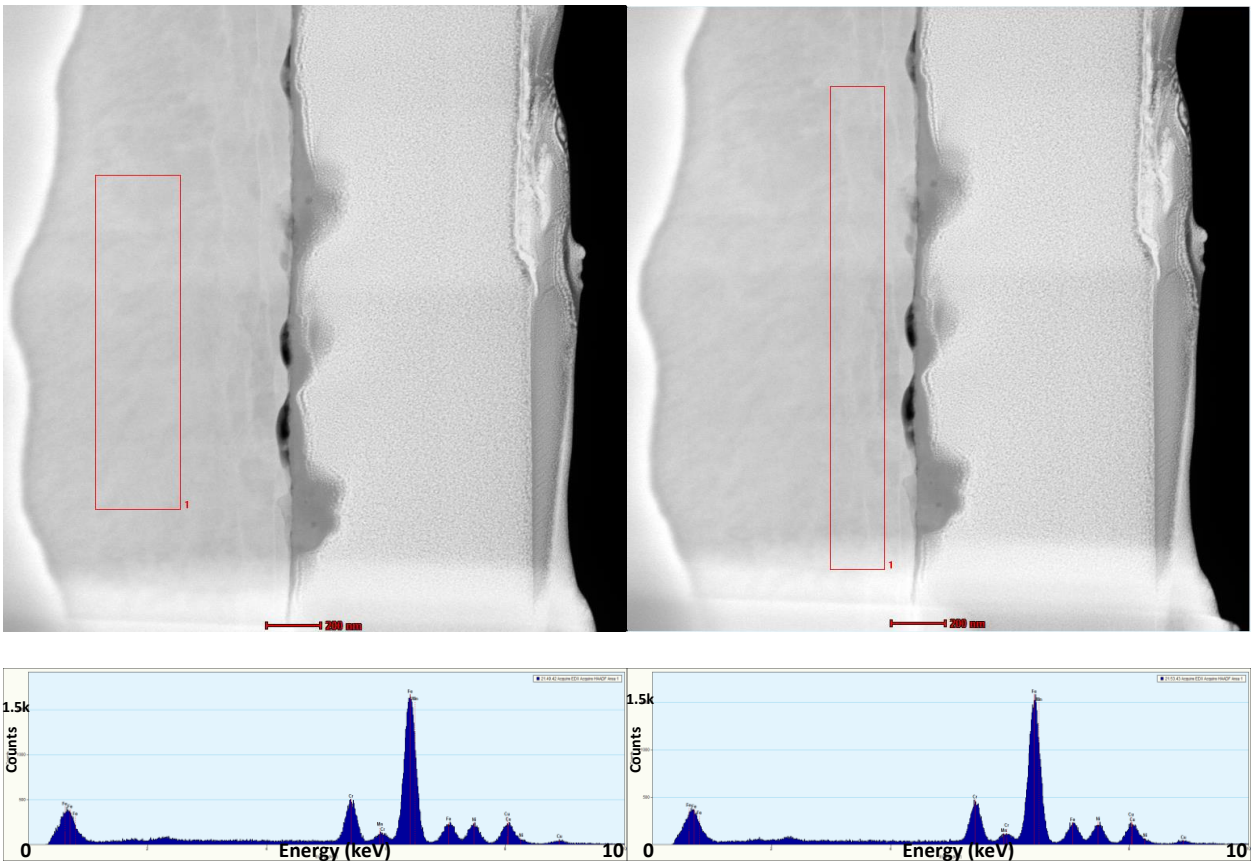


**Figure 3.28** STEM of Sample 3 substrate (left), subsurface (right) with EDX spectral signature. Energy ranges are 0-10 keV on horizontal axis.

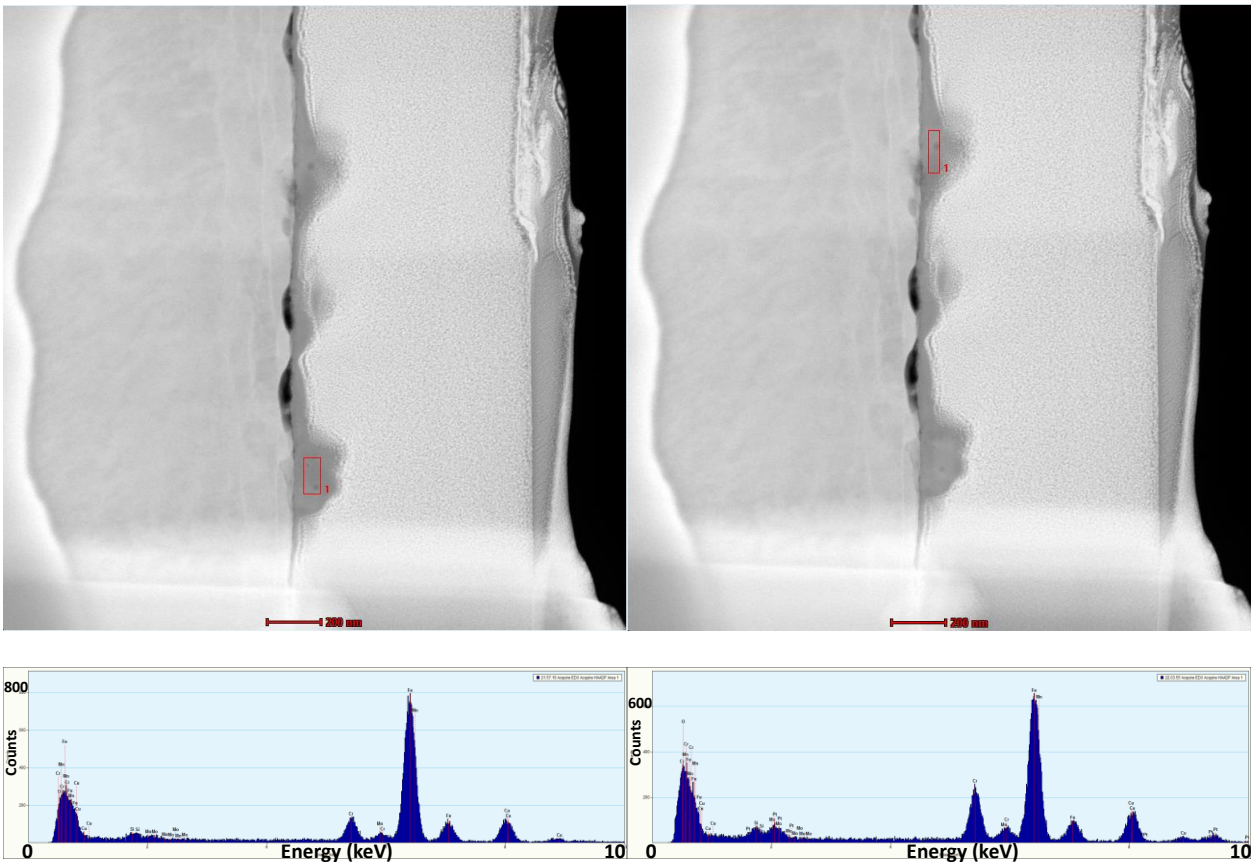


**Figure 3.29** STEM of Sample 3 large nodule (left), small nodule (right) with EDX spectral signature showing absence of nickel. Energy ranges are 0-10 keV on horizontal axis.

### 3.2.3 Control Sample STEM

The control sample shows a surface that is absent from surface "scale" or "slag", indicating that the surface features observed in the test samples are a consequence of the heat treatment. In Figure 3.30 we see the familiar substrate spectra.

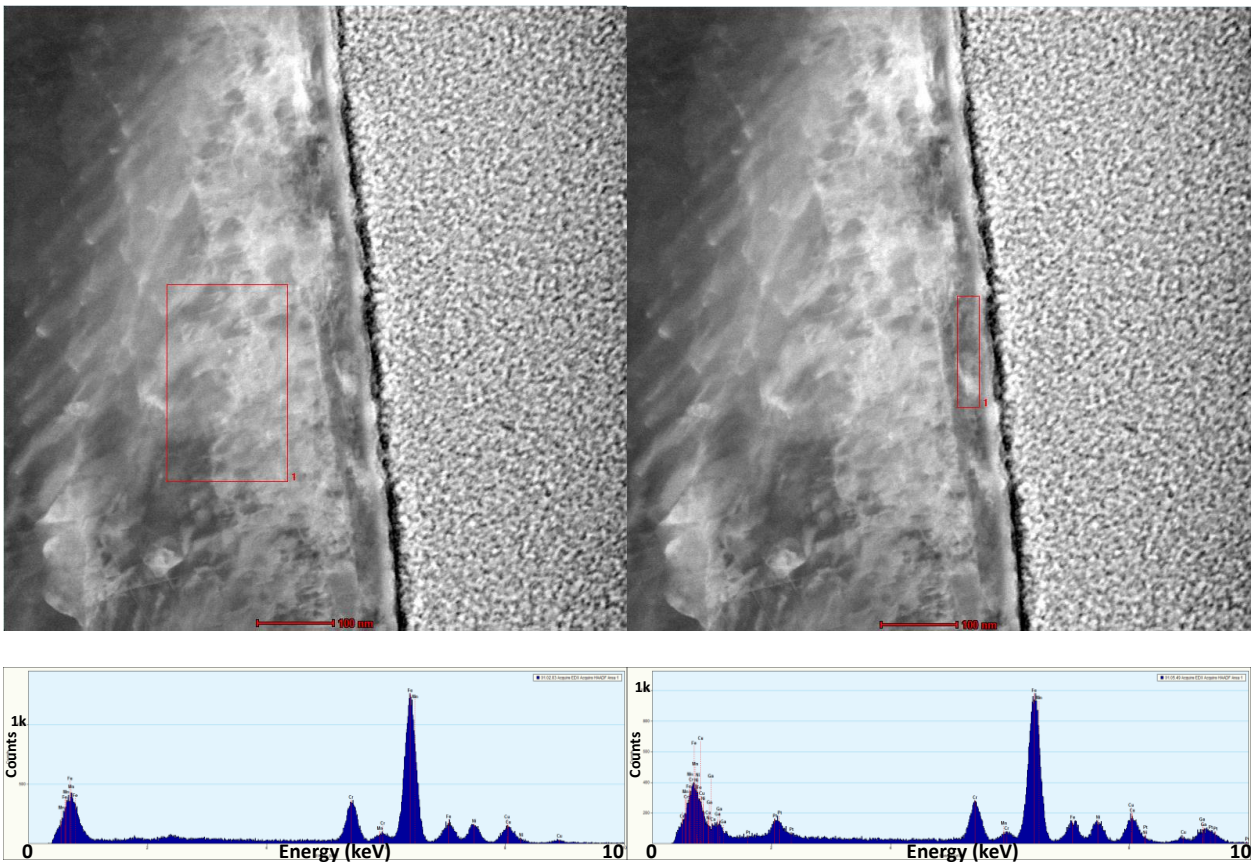


**Figure 3.30** STEM of control sample substrate (left), subsurface (right) with EDX spectral signature. Energy ranges are 0-10 keV on horizontal axis.

Figure 3.31 shows a line scan crossing the surface boundary. The signature remains consistent all the way to the surface. There is no drop in nickel and the dark line appears to be a gap between the surface of the steel and the deposited platinum. This appears to confirm that the material observed in the surface layer consists of Cr and Fe migration from the substrate onto the surface of the sample during the heat treatment.

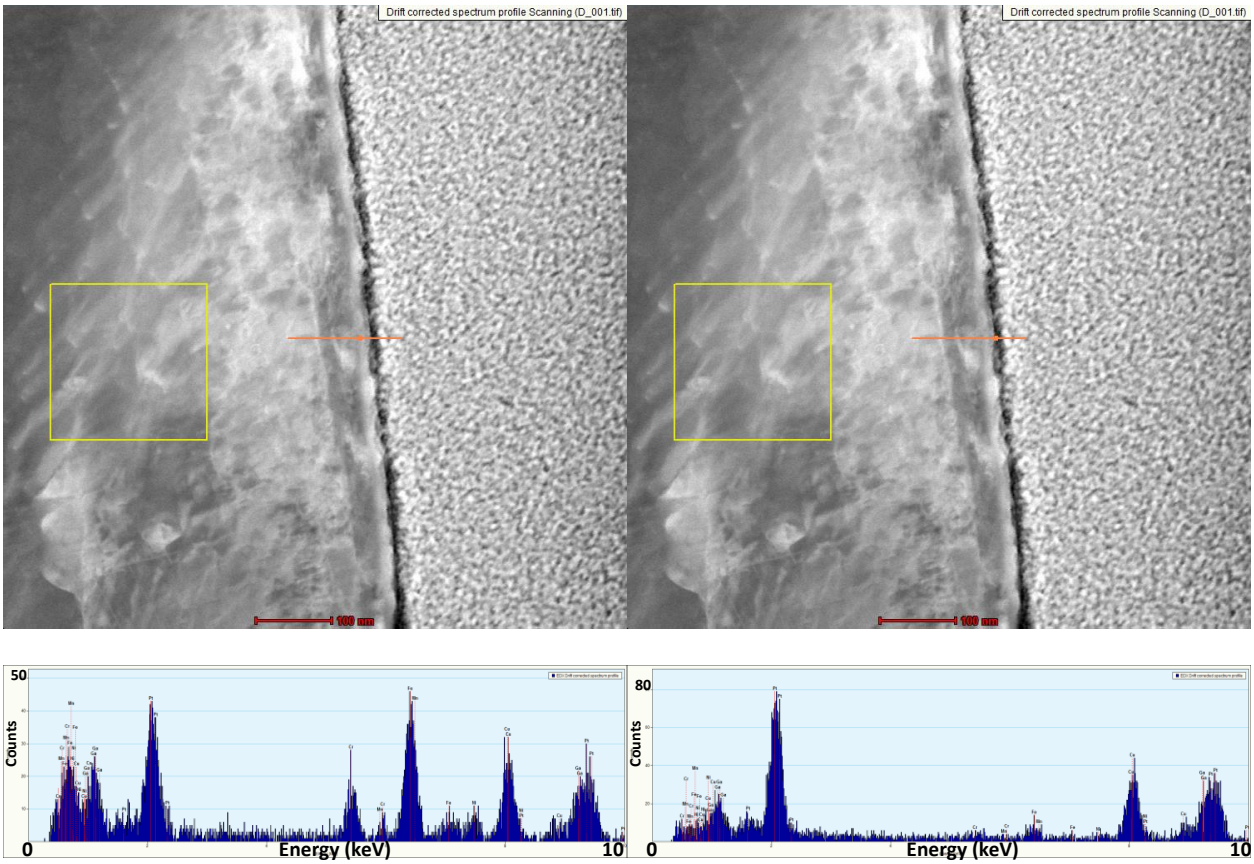


**Figure 3.31** STEM line scan of control sample. Subsurface (left), just below surface, showing nickel signature; gap (right), where counts are dominated by deposited platinum. Energy ranges are 0-10 keV on horizontal axis.

### 3.2.4 Sample 15 TEM

Sample 15, heat treated for 4 minutes in air and 15 in ethylene, shows carbon nanotube growth connected to regions of the surface layer. In Figure 3.31, we see the sample with TEM. There is an apparent reduction and further modification of the top surface layer that arises from the CNT growth processing. The mass-thickness contrast from the TEM indicates a denser surface layer that is no longer as continuous as observed prior to CNT growth. The carbon nanotubes are very light in color, indicative of low Z. There is a pronounced boundary between the substrate and subsurface, perhaps because of carbon infusion into the material.


**Figure 3.32** Sample 15 with TEM, showing substrate, surface layer and carbon nanotubes. The scale bars from left to right are 200, and 100 nm (respectively).

In Figure 3.33, the sample seen with STEM, the contrast is inverted, giving large Z material a light color. There is a distinct grain boundary between the top surface layer and the substrate. The speckled pattern on the nanotubes is likely due to redeposition during TEM sample preparation in the FIB.

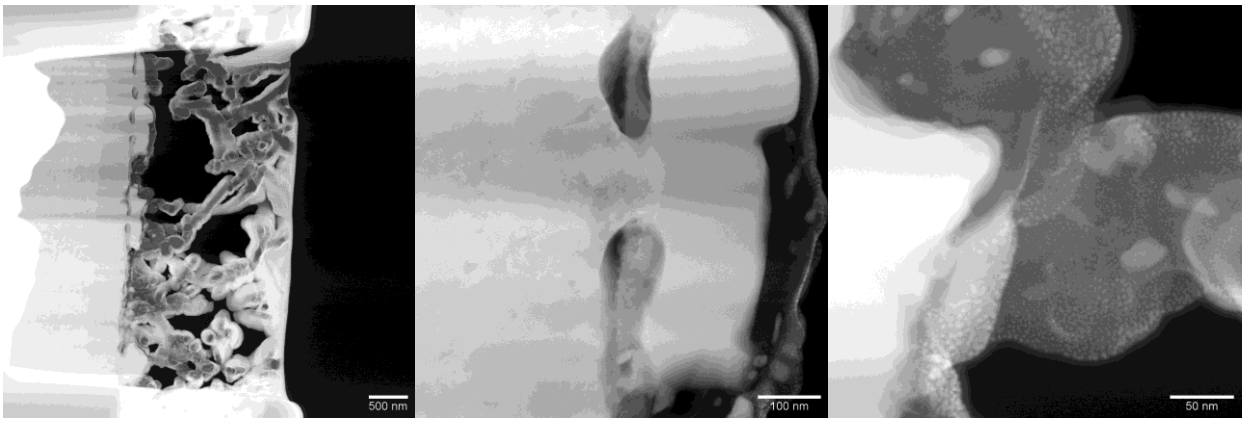


**Figure 3.33** Sample 15 with STEM, showing substrate, surface layer and carbon nanotubes. The scale bars from left to right are 500, 100, and 50 nm (respectively).

In Figure 3.34 we see a comparison of spectra taken at four different regions. The substrate and subsurface are very similar, with only a slight difference in the relative abundances of chromium and nickel. Chromium appears to rise slightly, while the nickel falls. At the boundary between subsurface and surface layer, the nickel drops away. This is further evidence of this material being the same layer that was observed in Samples 3 and 12, but now it has been reduced. Interestingly, the top surface layer, which used to be continuous, is now discontinuous and localized.

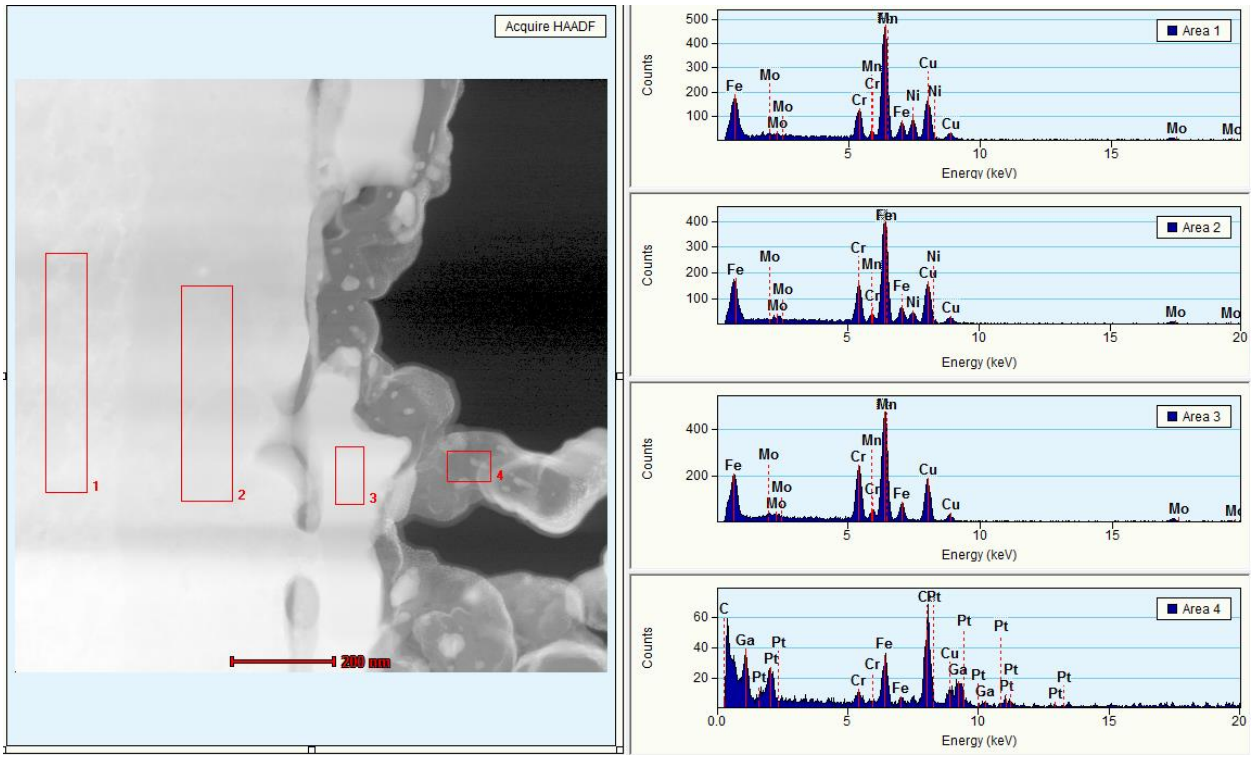


**Figure 3.34** Sample 15 with STEM, showing spectra of substrate, surface layer and carbon nanotubes.

## 3.3 Conclusion

Like the conclusions of previous work (Zhuo, 2014), we hypothesize that the source of the carbon nanotube growth on 316L stainless steel is reduced iron on or near the surface. Though this remains inconclusive. The stainless-steel surface appears to be modified by the heat treatment to produce a layer rich in chromium and iron oxides. Additionally, this formed surface layer appears to be reduced in the ethylene hydro-carbon atmosphere giving iron from which the CNTs can form.

Furthermore, the layer is shown not to be present in the original material, discounting the possibility that the surface layer seen after annealing was simply growth of what was already

there. The chromium and iron appear to have migrated to the surface, while leaving the nickel behind.

## 3.4 Recommendations

It is inconclusive as to the mechanism that catalyzes the CNT growth on stainless steel. This work brings forward several questions that remain unexplored. This section briefly outlines a selection of research areas that would benefit from further investigation.

### 3.4.1 Alumina coated CNT

In preparing the samples for TEM, much of the material was eroded by the FIB when doing the final thinning. If the sample was alumina coated, this may aid in preserving more of the material for analysis. This would also aid in finding areas where the carbon nanotube nucleation occurs.

### 3.4.2 Short CNT Growth

One avenue that may be very useful is the preparation and analysis of samples that have undergone very short CNT growth. The samples prepared for this thesis were exposed to ethylene for 15 minutes at 800°C. The CNT forests were too thick to allow a useful study of the surface. A much shorter heat treatment may capture the beginnings of CNT growth. Ideally, we would be able to find where carbon nanotubes are just beginning and be able to analyze the surface at these specific sites.

### 3.4.3 Oblique FIB Milling

Another strategy would be to use the ion beam to make a very oblique cut of the CNT forest. This would theoretically allow us to find more precisely the spot where the nanotubes

meet the surface. This in combination with alumina coating may allow us to precisely determine the nucleation site.

### 3.4.4 Scrape Test of Carbon Nanotubes

It is also of interest to conclusively determine that the growth that we are dealing with are carbon nanotubes and not simply carbon fibers. To determine this, scraping a sample to collect some of the fibers on a grid for use in the TEM would be useful.

# Appendix A

## Nodule Size Comparison chart

This appendix contains measurement data of the sizes of nodules on the surfaces of Sample 3 and 12.

Table 1. Table showing widths of selected nodules and their average (nm).

| Point | Sample 3 | Sample 12 |
|---|---|---|
| 1 | 194.895 | 220.564 |
| 2 | 167.655 | 237.469 |
| 3 | 145.545 | 176.485 |
| 4 | 172.041 | 166.518 |
| 5 | 145.545 | 176.485 |
| 6 | 163.419 | 210.533 |
| 7 | 190.421 | 197.944 |
| Average: | 168.503 | 197.9997 |

# Appendix B

## Heat Treated Stainless-Steel Samples

This appendix contains a list of samples and their respective heat treatment times in air, argon, ethylene, hydrogen.

Table 2. Heat-Treatment Times for Stainless-Steel Samples. Samples in bold-type had further EDX analysis done on them.

| Sample | Treatment Time | |
|---|---|---|
| | Air | Argon |
| Sample 1 | 1 | 0 |
| Sample 2 | 2 | 0 |
| **Sample 3** | 4 | 0 |
| Sample 4 | 1 | 5 |
| Sample 5 | 2 | 5 |
| Sample 6 | 4 | 5 |
| Sample 7 | 1 | 10 |
| Sample 8 | 2 | 10 |
| Sample 9 | 4 | 10 |
| Sample 10 | 1 | 20 |
| Sample 11 | 2 | 20 |
| **Sample 12** | 4 | 20 |

| Sample | Treatment Time | | | |
|---|---|---|---|---|
| | Air | Argon | Ethylene | Hydrogen |
| **Sample 13** | - | 20 | - | none |
| **Sample 17** | - | 20 | - | ramp up |
| **Sample 14** | 4 | 20 | 15 | - |
| **Sample 15** | 4 | 0 | 15 | - |

# References

Morco, S. (2021). Characterizing bacterial resistance and microstructure-related properties of carbon-infiltrated carbon nanotube surface coatings with applications in medical devices. *Theses and Dissertations,* https://scholarsarchive.byu.edu/etd/8909

Voss, S. (2021). Effects of carbon-infiltrated carbon nanotube growth on the biocompatibility of 316L stainless steel. *Theses and Dissertations,* https://scholarsarchive.byu.edu/etd/8913

Zhuo, C., Wang, X., Nowak, W., & Levendis, Y. A. (2014). Oxidative heat treatment of 316L stainless steel for effective catalytic growth of carbon nanotubes. *Applied Surface Science, 313*, 227-236. https://doi.org/https://doi.org/10.1016/j.apsusc.2014.05.189